photonics

MDPI

Article

Recent Advances in 850 nm VCSELs for High-Speed Interconnects

Hao-Tien Cheng [1], Yun-Cheng Yang [2], Te-Hua Liu [2] and Chao-Hsin Wu [1,2,*]

[1] Graduate Institute of Electronics Engineering, National Taiwan University, No. 1, Sec. 4, Roosevelt Rd., Taipei 10617, Taiwan; f06943156@ntu.edu.tw
[2] Graduate Institute of Photonics and Optoelectronics, National Taiwan University, No. 1, Sec. 4, Roosevelt Rd., Taipei 10617, Taiwan; r09941001@ntu.edu.tw (Y.-C.Y.); r09941030@ntu.edu.tw (T.-H.L.)
* Correspondence: chaohsinwu@ntu.edu.tw

Abstract: Vertical-cavity surface-emitting lasers (VCSELs) have made remarkable progress, are being used across a wide range of consumer electronic applications, and have particularly received much attention from the telecom and datacom industries. However, several constraints are thus currently being tackled to improve the device characteristics and modulation formats to meet the various demanding requirements of the future 800 GbE and 1.6 TbE Ethernet standards. This manuscript discusses the device characteristics and the key considerations in the device designs and optimizations. Finally, we elucidate the latest developments and vital features of modern 850 nm VCSELs for high-speed interconnects.

Keywords: high-speed optical interconnects; vertical-cavity surface-emitting lasers (VCSELs); 850 nm VCSELs; next-generation data communication VCSELs; modulation formats; 800 GbE; 1.6 TbE

Citation: Cheng, H.-T.; Yang, Y.-C.; Liu, T.-H.; Wu, C.-H. Recent Advances in 850 nm VCSELs for High-Speed Interconnects. *Photonics* **2022**, *9*, 107. https://doi.org/10.3390/photonics9020107

Received: 6 January 2022
Accepted: 6 February 2022
Published: 13 February 2022

1. Introduction

Since the invention of the VCSEL by Iga's group in 1978 [1,2] and the demonstration of its first room-temperature (RT, 300 K) operation in 1988 [3], many groups have continued to improve the technology to make the modern oxide-confined VCSEL. VCSELs offer several inherent advantages, such as monolithic fabrication, excellent beam quality, fast modulation bandwidth, and scalability in the forms of arrays. The incorporation of distributed Bragg reflector (DBR) mirrors and miniature microcavity designs [4,5] reduces the threshold gain and provides inherent mode selectivity. These approaches make VCSELs have very low thresholds (<2 mA) and efficient light sources [6]. The idea of putting active materials sandwiched between passive DBR mirrors is the prototype of the modern VCSELs. VCSELs have been used in a wide range of consumer electronic applications, industry applications, and sensing applications, and they have particularly attracted a lot of attention from the datacom industries.

Optical transceivers based on 850 nm VCSELs have been heavily used in short-reach interconnects in the datacom and telecom markets. The VCSEL market is projected to more than double to reach USD 20.9 billion by 2026 with heavy demand from new datacenters predicted by the market research reports from Yole Développement in 2021 [7].

This manuscript intends to provide an overall review on the latest developments and critical considerations in the design and optimization of high-speed 850 nm VCSELs and to provide some insights into the developments and applications of next-generation high-speed 850 nm VCSELs.

2. Basic Concepts of VCSELs

2.1. Device Structure

A VCSEL is a surface-emitting semiconductor laser with an elementary structure of a small active region with a monolithic resonator for emitting light perpendicular to the laser chip; Figure 1 provides a conceptual illustration of a VCSEL device. Two DBR

mirrors—p-type DBR and n-type DBR mirrors—enclose the active region, generating light between the two mirrors and forming an optical cavity, i.e., a laser resonator.

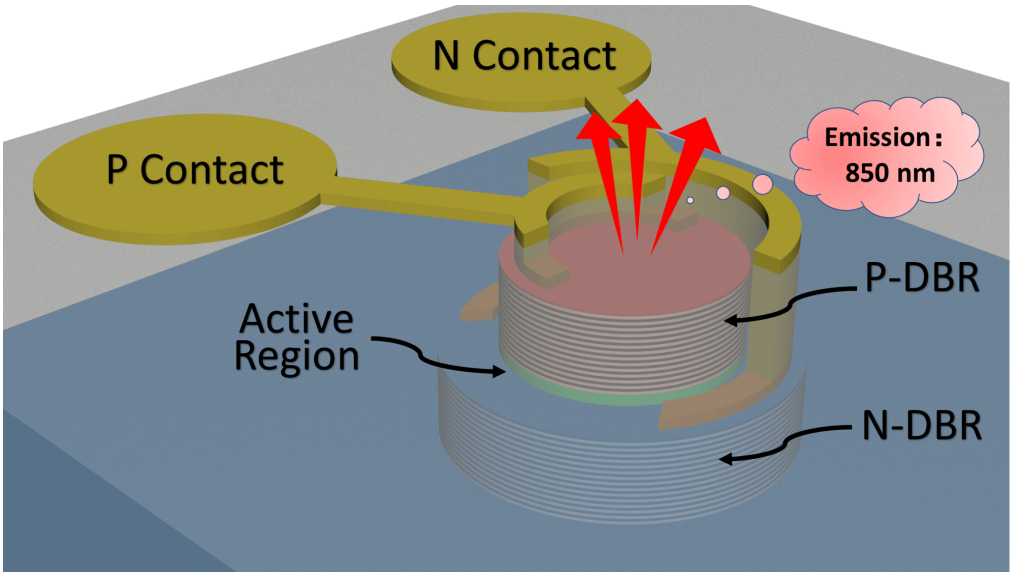

Figure 1. Schematic top view of an oxide-confined mesa-type VCSEL.

A cross-sectional view of the epilayer structure of a VCSEL is illustrated in Figure 2. Each VCSEL consists of two DBR mirrors parallel to the wafer surface. DBR mirrors usually consist of graded semiconductor layers of different alloys or compositions. The common candidates for DBR pairs are Al_xGa_yAs/Al_xGa_yAs for 850∼980 nm VCSELs and InP/AlGaInAs or InP/InGaAsP for 1300∼1550 nm VCSELs. While semiconductor DBR mirrors are preferred due to the ease of monolithic fabrication, metal mirrors, which can also serve as metal contacts (i.e., Au/Ag, Au/Ge), dielectric mirrors (i.e., SiO_2/TiO_2), and high-contrast grating (HCG) mirrors are also used. The reflectivities of the DBR mirrors are positively correlated to the number of pairs of DBR layers, and the light is emitted from the sides with lower reflectivities. Hence, VCSELs can be constructed in either top- or bottom-emitting configurations.

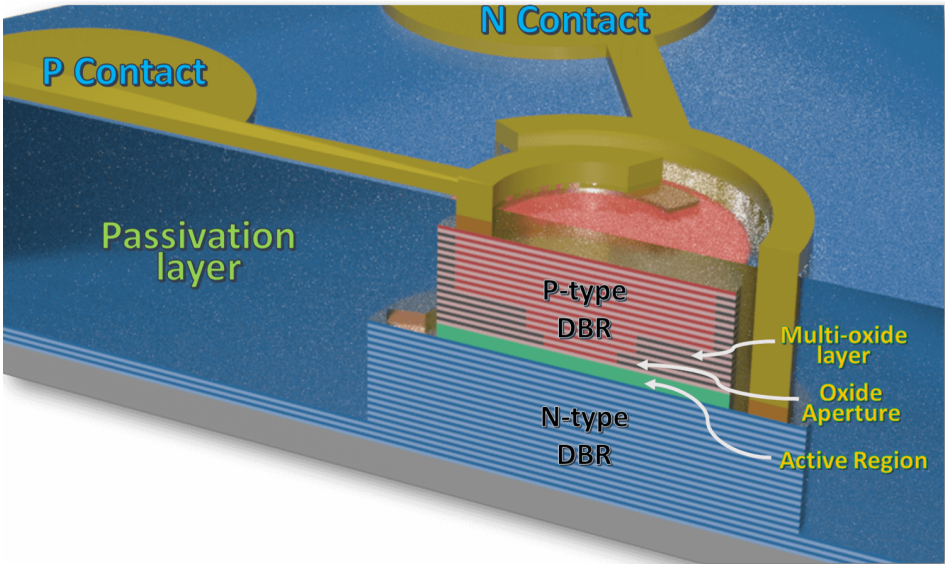

Figure 2. Schematic cross-sectional view of an oxide-confined mesa-type VCSEL.

The $Al_xGa_{1-x}As$ alloy offers a high-quality lattice-matched GaAs/AlGaAs material system for the formation of the DBR mirrors for 850 nm VCSELs. The high-Al-content

AlGaAs layers can be selectively oxidized to become stable native oxide (Al_xO_y) at higher processing temperatures and can be used for the formation of the current and optical confinement layers [8–10]. Additionally, the GaAs/AlGaAs layers offer good electrical and thermal conductivities [11].

The active region enclosed by the two DBR mirrors consists of multiple-quantum wells (MQWs), and the common choices are GaAs/AlGaAs and InGaAs/AlGaAs. Strained InGaAs/AlGaAs is more commonly employed for high-speed applications due to the improved optical gain and differential gain [12,13]. The separate confinement heterostructures (SCHs) provide enhanced optical and carrier confinements in the optical cavity [14].

The p- and n-type contact metals may be positioned either on the same face (both positioned on the top surface) or with the the top- and bottom-contact approach (with the n-type contact positioned on the back of the n-type doped substrate). The majority of modern high-speed VCSELs are oxide-confined, where the oxidation confinement layer is responsible for the current- and lateral-mode confinements. Oxide-confined VCSELs may be shaped into mesa- or trench-type structures to restrict the current flows and suppress the higher-order transverse modes. Mesa-type structures have the advantage of simpler processing. Trench-type structures are usually preferred for large-volume processing, as trench-etching processes have better control than that of mesa-etching processes. The etched regions around the mesas or the trenches are usually filled with materials such as dielectrics (e.g., SiN [15]), polymers (e.g., polyimide [16,17], benzocyclobutene (BCB) [17–19]), or metals (e.g., Al) [20].

2.2. Pros and Cons of VCSELs

VCSELs have surface-emitting characteristics that make them radiate emissions perpendicular to the wafers, as opposed to most other semiconductor lasers, where light is emitted at one of the edges of the laser chip. VCSELs are different laser technologies that offer some advancements while also having some setbacks.

2.2.1. Pros

These surface-emitting features allow them to have enhanced beam qualities and circular light beams that can be easily scaled and incorporated in large quantities into 2D arrays of VCSEL chips. Additionally, only a single longitudinal mode can exist due to having much shorter cavity lengths (typically $\leq 2\lambda$ long). Hence, VCSELs do not suffer from kinks in the optical light–current (L-I) curves as some other semiconductor lasers do when their power switches to other modes at different current injections.

Apart from enhanced beam qualities and fast modulation bandwidths, VCSELs hold leading positions due to the lower cost of processing, scalability into arrays, thermal stability (i.e., wide operating temperature range) [21–23], wavelength stability [22,24], etc.

2.2.2. Cons

One of the main limiting factors of VCSELs is the relatively small output power (usually ≤ 10 mW for a single device) due to the small active regions. VCSEL developers have been facing the challenges of increasing the total power output of single VCSEL devices. Drummer et al. from Vixar Inc. published their VCSEL with a multi-junction active design and reached $\geq$60% power conversion efficiency (PCE) with three- and five-junction VCSELs [25].

VCSELs usually have relatively higher series and thermal resistance, thus lowering the operating currents and causing severe negative impacts on high-speed performance. It is important to note that VCSELs often have a certain degree of polarization instabilities at various current injections due to the lack of mechanisms for selecting specific polarizations.

2.3. Applications of VCSELs

VCSELs are commonly used in several areas in high-speed optical communications, sensing, autonomous vehicles, data storage, computing, etc. Some of the key applications of VCSELs are shown in Figure 3.

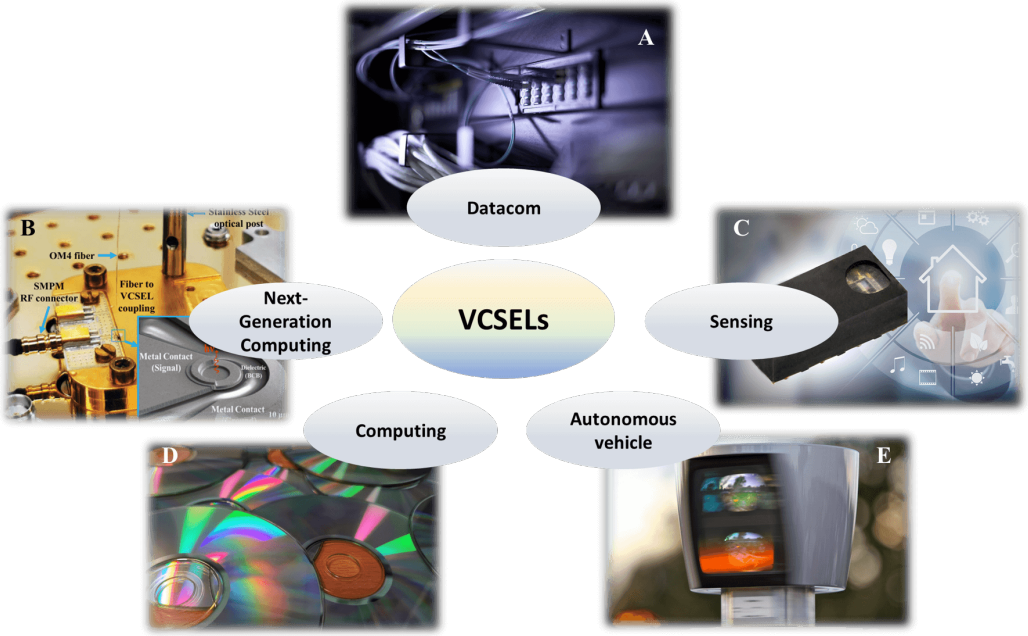

Figure 3. Various Applications of VCSELs: (**A**) Fibers in data centers [26]; photo by CommScope (Creative Commons Attribution CC BY license). (**B**) Packaged high-speed cryogenic VCSEL chip with the device's SEM image (inset); reprinted with permission from [27], Copyright © 2021 AIP Publishing LLC. (**C**) VCSEL-Powered VCNL36826S proximity sensor for consumer and industrial applications [28]; photo by Vishay Intertechnology (Creative Commons Attribution CC BY license). (**D**) Optical storage mediums. (**E**) A Velodyne HDL-64E LiDAR [29,30]; photo by Jurvetson (flickr) (Creative Commons Attribution CC BY license).

2.3.1. Datacom

The high-speed characteristics of VCSELs enable them to be widely used in transceivers or active optical cables (AOCs). In 2002, the Institute of Electrical and Electronics Engineers (IEEE) defined Std. P802.3ae for 10 GbE [31]. The 100GBASE-SR4 was standardized in IEEE Std. P802.3bm using four 25 GbE VCSEL optical lanes for 100 GbE applications in early 2015 [32]. In 2017, the IEEE Std. P802.3bs standardized the 400GBASE-SR16 using 16 optical links with 25 Gb/s per optical channel for an Ethernet link of 400 GbE [33]. In 2020, the 400GBASE-SR8 was defined to double the individual channel data rates to 50 Gb/s in IEEE Std. P802.3cm [34]. In 2020, the Ethernet Alliance envisioned the future Ethernet speed to reach 800Gb/s and 1.6Tb/s in their Ethernet Roadmap 2020 [35].

2.3.2. Sensing

Various industry sectors apply VCSEL-based light sources in gas, biomedical sensing, and consumer-market products, such as facial and gesture recognition systems. Wavelength-tunable VCSELs, which are usually manufactured with microelectromechanical systems (MEMS), are used to measure the types of gaseous molecules. Biomedical and industrial sensing is starting to adopt VCSELs as integrated light sources for medical diagnostics, imaging, and sensing technologies.

2.3.3. Autonomous Vehicle Systems (AVSs)

Light-detection and ranging (LiDAR) technologies can create 3D mappings using laser beams to scan their surroundings. The most common sensors in AVSs are cameras,

radars, and LiDAR. In the meantime, LiDAR technology has been adopted by the majority of self-driving companies—most notably, self-driving car project subsidiary owned by Alphabet Inc., Waymo [36]. In the meantime, VCSEL-based sensing systems use LiDAR and time-of-flight (ToF) technologies to provide long-range proximity- and distance-sensing applications. Commercial LiDAR manufacturers, such as Velodyne, developed a LiDAR prototype for AVS back in 2005, which eventually became one of the early LiDAR products, the Velodyne HDL-64E [29,30].

2.3.4. Computing

VCSELs can also be applied in low-cost light source solutions for tracking movement in computer mice, defining the images in laser printers, and transferring data with optical storage mediums, such as CDs and DVDs [37]. Xerox was one of the earlier pioneers in laser printing and designed a VCSEL-ROS system for laser printing with high-resolution, vibrant color images [38].

2.3.5. Next-Generation Computing

Over the last few years, quantum computing has been the focus of various researchers, and quantum wiring is one of the most problematic issues at below 4 Kelvin (K) or even milliKelvin (mK) levels of cryogenic environments [39]. VCSELs have shown their capabilities in cryogenic environments and have been operated up to 40 and 50 GHz, as reported by Cheng et al. and Feng's group at the University of Illinois Urbana-Champaign (UIUC) in 2020 and 2021, respectively [40,41]. For readout circuits that usually operate at sub-4K, Feng's group demonstrated a cryo-VCSEL that may operate at an extremely low temperature of 2.6 K with an error-free transmission of up to 12.5 Gb/s [27].

3. Evolution of High-Speed 850 nm VCSELs

The first small form-factor pluggable (SFP) transceivers supported only up to 100 Mb/s and 1 Gb/s when they were introduced in the market in 2001 [42]. Several years later, SFP+ and SFP28 transceivers were developed to carry data rates of 10, 25, and 28 Gb/s [43,44]. QSFP+ transceivers integrate four transmitters and four receivers to support a 40 GbE link [45]. QSFP28 supports quadruple lanes, but differs in "28", as the name says, with each lane carrying data rates of up to 28 Gb/s and combined into a single 100 GbE link [46].

In order to support the modern 200 and 400 GbE or even the future 800 GbE and 1.6 TbE Ethernet standards using optical interconnects [47,48], the current VCSEL designs and manufacturing technologies must be improved to support single lanes with faster data rates.

3.1. Various Signal Modulation Formats

While the industry has been focusing on extending the 3 dB modulation bandwidths of laser devices, the development and adoption of advanced new modulation formats are also essential for enabling more efficient use of the channel bandwidths. In this section, various signal modulation formats for VCSEL optical links are described and explained, and their capacities for increasing the channel bandwidth densities are discussed.

There are three main ways to increase optical data rates:

1. Channel frequency:
Increase the optical channel frequencies of the optical modulators.
2. Parallelism:
Increase the number of channels by either increasing the number of fibers or using multiple wavelengths in a single fiber, which is known as wavelength-division multiplexing (WDM). Technologies such as frequency-division multiplexing (FDM) also allow more efficient use of the channel modulation bandwidth.
3. Complexity:
Increase the number of bits per symbol by incorporating various advanced modulation formats.

Modulation formats are simply the languages that transmitters and receivers speak to communicate. The goal of these modulation formats is simply to transmit data over data links (which may be coaxial cables, fibers, or PCB traces). High-speed datacom VCSELs and fibers act as analog baseband channels (also known as low-pass channels) and allow transmission of data signals using analog or digital modulation methods.

The commonly used modulation formats by the datacom and telecom industries are illustrated in Figure 4. Some sophisticated and advanced modulation formats have the advantage of offering higher data rates with the same laser devices. However, these formats usually put more demanding requirements on the light sources.

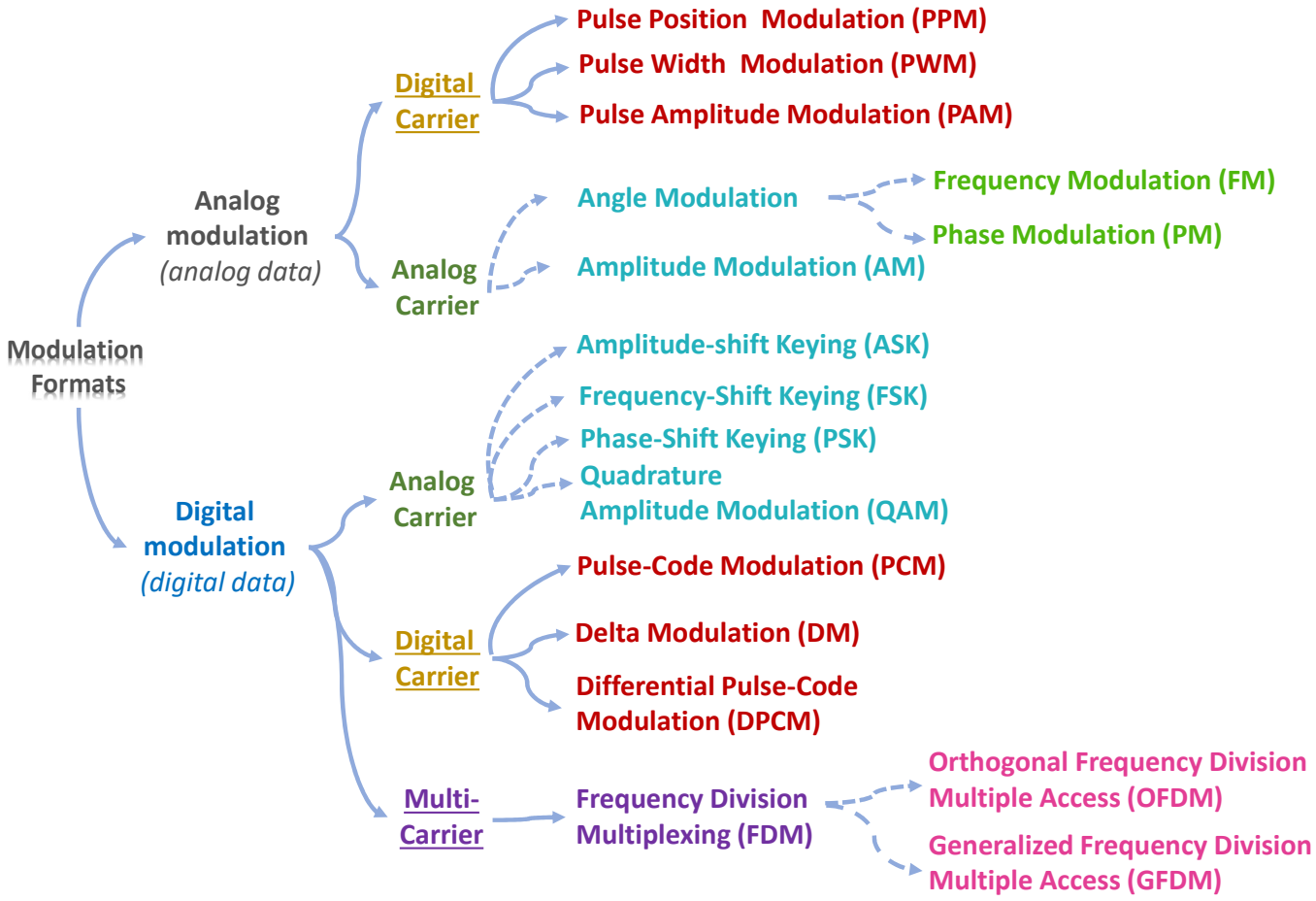

Figure 4. Categorization for signal modulation based on data and carrier types.

Advanced modulation formats with multi-level and multi-carrier modulation technologies have been developed to reduce the interconnect bandwidth requirements [49]. These formats are gaining traction to become some of the next-generation VCSEL-based Ethernet standards in IEEE Std. P802.3 bs and P802.3 cm [33,34]. With an eye toward increasing the transmission capacity of the data links, advanced modulation formats, such as pulse amplitude modulation (PAM) [50,51], and quadrature amplitude modulation (QAM) [52–54] (including various variants, including carrier-less amplitude and phase modulation (CAP)), and FDM (including various variants, such as orthogonal frequency-division multiplexing (OFDM) [50,55–57], generalized frequency-division multiplexing (GFDM) [58], and discrete multi-tone (DMT) [49,54]) are being developed to meet the datacom and the telecom industries' requirements [52].

3.1.1. Non-Return to Zero (NRZ)

NRZ, also called PAM-2, is a two-level pulse amplitude modulation using binary codes of high and low signal levels to represent the zeros and ones of digital signals, and it is one of the most commonly used modulation formats. One single bit of logic information (0 and 1) can be transmitted per period of the clock period. The Nyquist frequency of an NRZ signaling is half of the transmitted data rate (e.g., a 56 Gb/s NRZ signal has a Nyquist frequency of 28 GHz).

In 2018, Wu et al. demonstrated a VCSEL device that enabled an error-free transmission of up to 50 Gb/s at BtB [59]. In the following year, Huang et al. demonstrated 54 Gb/s error-free BtB transmission, as shown in Figure 5 [60]. In 2021, Chorchos et al. from VI Systems GmbH (VIS) and the Warsaw University of Technology (WUT) reported a record 80 Gb/s using feed-forward equalization (FFE) technology with a 30 GHz VCSEL and BiCMOS driver packaged into a 33 GHz transceiver [61]. The latest reported 3 dB modulation bandwidth of an 850 nm VCSEL at RT was ~30 GHz [22,61–65], as they were close to the bandwidth limits of the VCSEL's intrinsic responses. For more efficient use of the VCSEL modulation bandwidths, the industry has moved toward other advanced modulation formats for 400 GbE, 800 GbE, and 1.6 TbE [35].

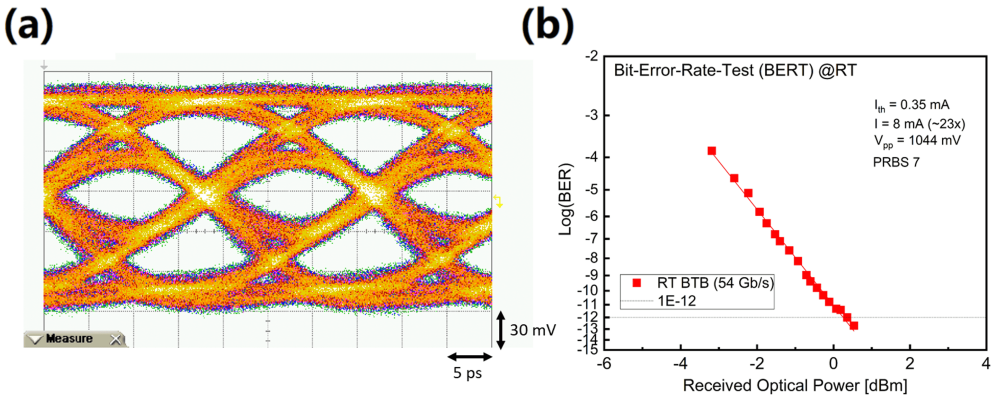

Figure 5. (**a**) The NRZ eye diagram and (**b**) the bit error rate (BER) at 54 Gb/s with the VCSEL demonstrated by Huang et al.; reprinted with permission from [60], Copyright © 2019 IEEE.

3.1.2. PAM-4

Due to the limited channel transmission bandwidths, multi-level modulation formats could be used to reduce the Nyquist frequency requirements of the optical channels. PAM-4 is a four-level modulation format that uses four signal levels for signal transmission. Two bits of information (00, 01, 10, and 11) can be transmitted within each clock period, and they allow the doubling of the channel data rate using the same optical channels. Therefore, PAM-4 requires 1/2 of the Nyquist frequencies for the same data transmission rates compared to NRZ, resulting in fewer channel-dependent losses due to the limited bandwidths of the light sources. This provides a doubling of the transmission efficiency and reduces the transmission cost, and PAM-4 has been selected to be used in transceivers and jacked-up connection speeds for the 200 and 400 GbE Ethernet [32,34,66].

PAM-4 signals have tighter spacings between signal levels and only possess 1/3 of the amplitude of NRZ signals under identical modulation voltages. Therefore, PAM-4 signals are at least three times more sensitive to the channel noises, and the non-linear responses of VCSELs would put heavier burdens on the optical channels. Therefore, PAM-4-based transceivers have to be comprised of more sophisticated circuits and are usually more power-hungry than NRZ-based transceivers to compensate for the more stringent signal-to-noise (SNR) requirements [67].

In 2020, Huang et al. demonstrated up to 84 Gb/s (42 GBd) PAM-4 operation with a high-speed VCSEL, as shown in Figure 6 [50]. Error-free transmission channels with PAM-4 require clear openings of the three "eyes". As shown in Figure 6b, the three "eyes"

in PAM-4 suffer from different BERs, and the top and bottom eyes are usually heavily contested with the reduced signal spacings. In 2020, Lavrencik et al. from the Georgia Institute of Technology (GIT), VIS, and WUT demonstrated a record 168 Gb/s (84 GBd) PAM-4 operation with 28 GHz VCSELs [51].

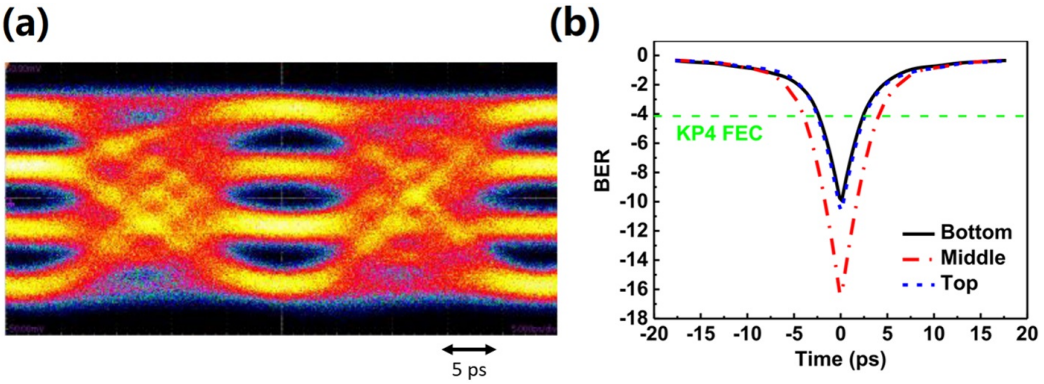

Figure 6. (**a**) The PAM-4 eye diagram and (**b**) the receiving BER at 42 GBd with the VCSEL demonstrated by Huang et al.; reprinted with permission from [50], Copyright © 2020 IEEE 2020 (Creative Commons Attribution CC BY license).

3.1.3. QAM

QAM is a family of digital modulation methods that consist of two signals, which may be in either analog or digital format. The common systems are the analog QAM system in NTSC and PAL television systems and digital QAM systems for telecommunications systems, such as IEEE P802.11 WiFi. QAM transmits two out-of-phase signals that contain both amplitude and phase variations, and it effectively transmits two PAM signals using carriers of the same frequency, but in phase and quadrature. Hence, QAM signals occupy only half the bandwidth required, as compared to PAM signals. In 2016, Puerta et al. demonstrated a 107.5 Gb/s multi-band approach to CAP with combinations of QAM and PSK modulations using SM-VCSEL in a 100 m OM4 multi-mode fiber (MMF) link [53]. In 2021, Ledentsov et al. from VIS, WUT, and Fraunhofer HeinrichHertz Institute (FHHI) demonstrated BtB modulation records with up to 224 Gb/s with 850 nm VCSELs and 219 Gb/s with 910 nm VCSELs. Ledentsov et al. used 4-QAM DMT and some receiver signal processing techniques, including signal down-sampling, low-pass filtering, CP removal, FFT, an equalizer for each subcarrier, parallel-to-serial conversion, BER/EVM (error vector magnitude) estimation, and bitloading [54].

3.1.4. FDM

Multi-carrier modulation transmits data by splitting it into several smaller components and dispatching the data splits over separate carrier frequencies. The combined signal forms a broader bandwidth, while the individual carriers have much narrower bandwidths. This technology has been widely used in communications over channels with severely limited bandwidths, e.g., ADSL systems over telephone networks. The inclusion of these formats allows higher utilization rates for the optical channels and can support higher data rates per optical data link.

The common multi-carrier modulation formats used in datacom include various FDM variants, such as OFDM, GFDM, DMT, etc. GFDM has been proposed as the waveform for transmitting signals for the 5G standards, and it has also become the leading candidate waveform for the future 6G standards. These modulation technologies offer high utilization of the optical transmission channels and allow much higher channel modulation data transmission rates. In 2017, Kao et al. demonstrated up to 80 Gb/s with 16-QAM OFDM [55], as shown in Figure 7, and the same group further demonstrated an improved result of 140 Gb/s in early 2020 [50].

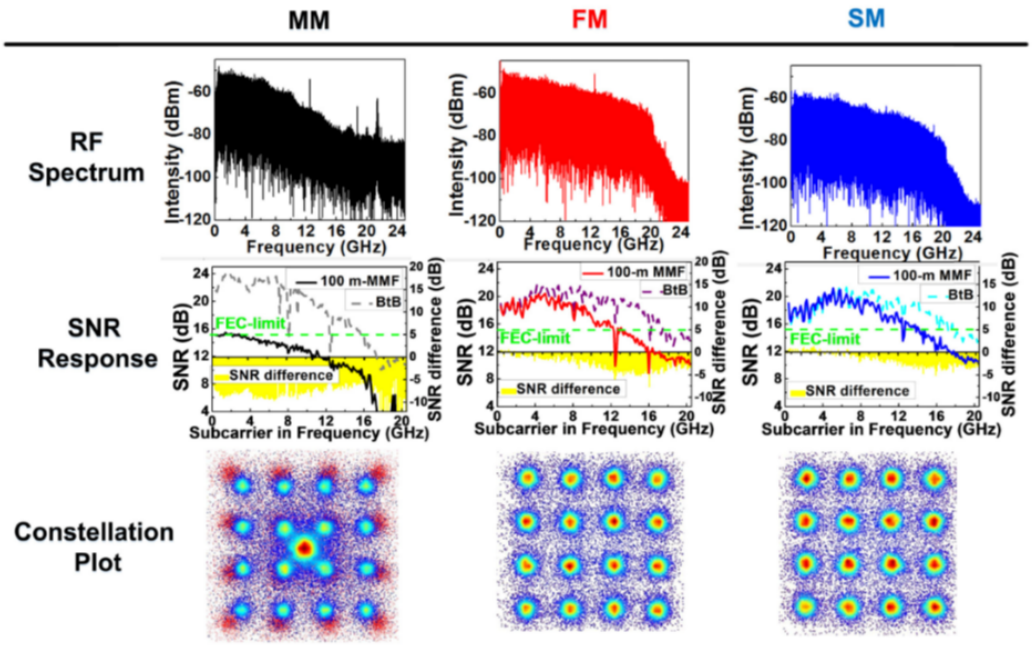

Figure 7. The RF spectra, SNR responses, and constellation plots of the 100 m MMF transmitting 80 Gbit/s data carried by the MM, few-mode (FM), and SM VCSEL chips, respectively; reprinted with permission from [55] © The Optical Society.

3.2. Mode Control

Apart from the power attenuation in fibers over long distances, the dispersion effects may significantly deteriorate the transmission qualities over long-reach interconnects. The dominant dispersion effects in optical fibers are modal dispersion and chromatic dispersion [68]. The ray-optics analogy portrays that lights may enter the fibers at different angles and travel on different paths. Consequently, signals arrive at the other ends of the fibers at different times, causing modal dispersion. VCSELs obtain single-longitudinal-mode operation due to their short optical cavities, but operate in multiple transverse modes depending on the aperture sizes. These multiple transverse modes may transmit at different velocities in the fibers and cause the occurrence of chromatic dispersions. Additionally, the issues of chromatic dispersions, power losses, and mode delays also prevail and significantly impair the transmission qualities of long-reach optical links with MM VCSELs [68].

According to experimental and calculated results, SM VCSELs offer a significantly superior system reach compared to MM VCSELs and relieve the reliance on additional digital signal processing (DSP) to compensate the dispersion and relative intensity noise (RIN)-related noises in the optical channel [68–72]. The use of SM VCSELs allows the use of single-mode fibers (SMFs), which offer slightly improved long-range transmission reaches, as shown in Figure 8a [68]. Additionally, FM VCSELs and SM VCSELs have reduced linewidth, thus offering longer system reaches, as illustrated in Figure 8b [68]. The spectral bandwidth (RMS) requirement for 100GBASE-SR4 was standardized to $\leq$0.6 nm, as defined in IEEE Std.P802.3cm [34], while using light sources with smaller spectral widths may allow longer transmission distances, as 10GBASE-SR defined in IEEE Std. P802.3ae, for up to 300 m transmission in fibers [31]. There have been reports that using FM VCSELs with RMS spectral widths of $\leq$0.3 nm may support longer-distance transmissions [68,73], which are consistent with the calculated results [68].

Kao et al. compared MM, FM, and SM VCSELs with different oxidation aperture sizes and emission spectra, and investigated their influences on the laser modes over 100 m MMF in 2017, as illustrated in Figure 9 [69]. Chromatic-dispersion-free SM VCSELs offer even more superior performance in long-reach-transmission links. Qiu et al. reported a 1000 m optical link with error-free transmission at up to 28 Gb/s in 2019 [70]. Peng et al.

demonstrated a 500 m optical link with up to a record 40 Gb/s without equalization with a homemade SM VCSEL in 2020, as shown in Figure 10 [71].

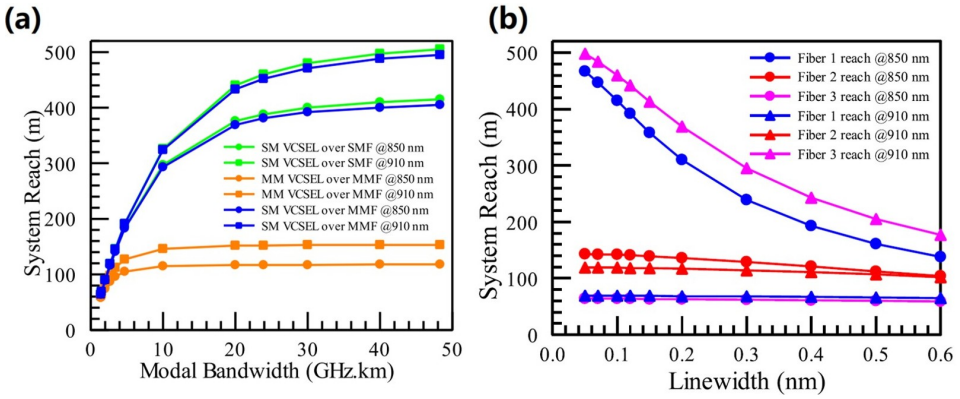

Figure 8. (**a**) Comparison of the calculated results of the system reach of an SM VCSEL over SMF, an SM VCSEL over MMF, and an MM VCSEL over an MMF transmission system as a function of the fiber modal bandwidth at 850 and 910 nm; (**b**) the impact of the laser linewidth of SM VCSELs on the system reach using the three fibers; reprinted with permission from [68], Copyright © 2021 IEEE.

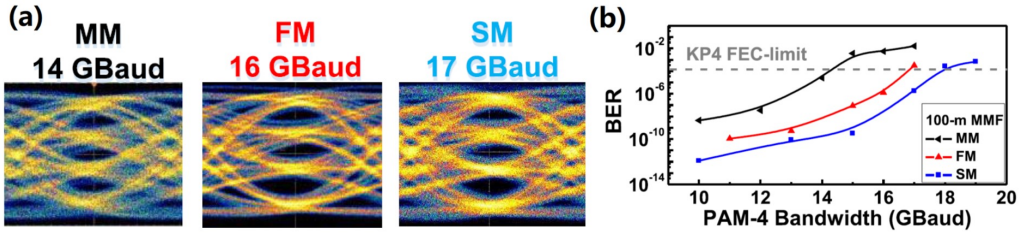

Figure 9. MM, FM, and SM VCSELs transmitting over a 100 m MMF; (**a**) PAM-4 eye diagrams; (**b**) BERs at 14, 16, and 17 GBd, respectively; reprinted with permission from [69], Copyright © 2017 IEEE.

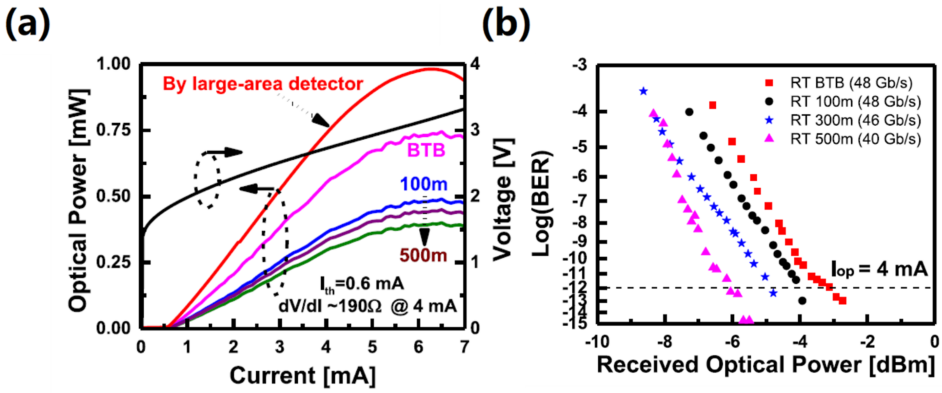

Figure 10. (**a**) Light–current–voltage (L-I-V) characteristics of an 850 nm SM oxide-confined VCSEL fabricated by Peng et al. (**b**) The BERs versus receiver powers through different lengths of OM4 fiber (48 Gb/s over BTB and 100 m, 46 Gb/s over 300 m, and 40 Gb/s over 500 m OM4 MMF); reprinted with permission from [71], Copyright © 2020 IEEE.

Various process techniques have been used for the suppression of the higher-order modes. The typical process techniques that reduce the transverse modes are the implantation process for the formation of current-blocking layers [74] and the oxidation layers formed by the native oxides of AlGaAs alloys for the current and optical confinements [8–10]. Oxide VCSELs with oxidation apertures have become the common industry practice for the current and mode controls [10]. Other mode-suppression techniques include surface relief [75,76], photonic crystals [77,78], impurity-induced disordering (IID) (also

referred to as Zn diffusion) [71,79–85], oxide relief [81,86], and integrated mode-selective filter (iMSF) structures, which induce losses of the higher-order modes [70,87], as well as lithographic VCSELs with a phase-shifting mesa (PSM) [88,89].

However, SM VCSELs are still not commercially feasible, as the manufacturing techniques are usually complicated and costly, and their yield rates are not usually guaranteed. Moreover, SM VCSELs usually suffer from additional differential resistance, joule heating, higher failure rate, and poor reliability issues.

4. Design and Optimization of High-Speed 850 nm VCSELs

The design of VCSELs is rather complicated, as it requires a comprehensive design for both the electrical and optical properties of the epilayer structure. Technology Computer-Aided Design (TCAD) software is usually employed in the design process of the devices to optimize the epilayer design and the device structure design. TCAD can significantly accelerate the design process and reduce the expenses of multiple time-consuming and costly epitaxial wafer growths [90].

The winning formula for VCSELs is epitaxial DBR mirrors for providing excellent optical confinement, low resistivity, and optimized thermal design and optimally designed gain mediums for providing large gain and differential gain. These designs would provide enhanced intrinsic modulation responses. In the meantime, an adequately optimized optimization RC damping through the structural and layout design of the epilayer may offer large modulation bandwidths while providing sufficient damping to compensate for the intrinsic relaxation oscillations [91]. These damped microwave electrical-to-optical (E-O) responses may offer superior large-signal data transmission performance.

4.1. Transfer Functions

Due to the above-mentioned intrinsic and extrinsic influences in VCSELs, it is of utter importance to study the transfer functions of VCSELs and to investigate the design and optimization criteria. It is worth repeating that a VCSEL's overall E-O responses are the superposition of the intrinsic laser responses and the extrinsic electrical RC responses [14,21,92,93]. The overall E-O response of a VCSEL can be characterized by a three-pole transfer function, Equation (1), which is the superposition of the two-pole intrinsic and the one-pole electrical transfer functions [14,92]:

$$H(f) = H_{\text{intrinsic}}(f) \cdot H_{\text{electric}}(f) \tag{1}$$

where:

$H_{\text{intrinsic}}(f)$ = the intrinsic transfer function of VCSELs
$H_{\text{electric}}(f)$ = the electrical transfer function due to the RC parasitic roll-off

The carrier modulation mechanisms inside VCSELs determine the modulation bandwidths and the optical channel transmission rates. The intrinsic transfer function resembles a second-order filter that can be characterized by a two-pole equation [14]:

$$H_{\text{intrinsic}}(f) \equiv \frac{t(f)}{i_a} = A \cdot \frac{{f_R}^2}{{f_R}^2 - f^2 + jf(\gamma/2\pi)} \tag{2}$$

where:

A = the fitting constant
$t(f)$ = the optical modulation amplitude
i_a = the modulated current through the active region of the VCSEL, as illustrated in Figure 11
γ = the damping rate

The parasitic elements in VCSELs can be characterized by measuring the input reflection S_{11}, which is measured by a vector network analyzer (VNA). The RC parasitic damping can be described by a one-pole transfer function with a pole at f/f_P that limits

the modulation responses of VCSELs. The electrical transfer function can be characterized by a one-pole transfer function:

$$H_{\text{electric}}(f) = \frac{1}{1 + j(f/f_{\text{P}})} = \frac{i_{\text{a}}(f)}{i_{\text{tot}}(f)} \cdot (1 - S_{11}) \tag{3}$$

where:

f/f_{P} = the extra pole that resembles the RC parasitic roll-off

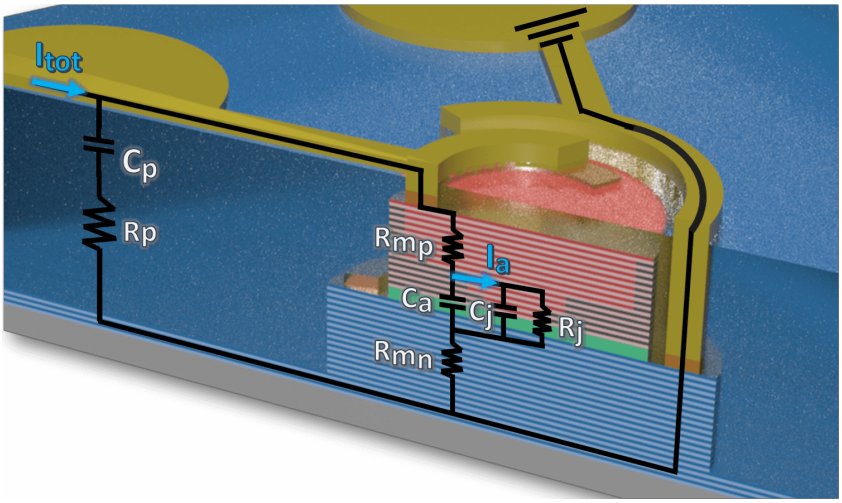

Figure 11. The small-signal equivalent circuit model of an oxide-confined mesa-type VCSEL.

4.2. Active Region Design

The physical mechanisms governing VCSELs and other semiconductor lasers are essentially correlated to the current injections and carrier recombinations in the active regions of the VCSELs [14]. The designs of the active regions (including the MQWs, barriers, SCHs, etc.) have significant primary influences on the steady-state and dynamic responses of VCSELs [94]. The optical gain dramatically depends on the optical and carrier confinement in the laser cavity.

The design and selection of materials for the active regions heavily influence the static and dynamic performances of VCSELs, and high-speed VCSELs favor high differential gains and low lasing thresholds [24]. The active region of VCSELs is typically formed by MQWs sandwiched by SCHs, and the cavity gain of VCSELs is usually limited by a short resonator round-trip time in the optical cavity. Hence, the MQWs are usually placed at the nodes of the optical field to reduce the lasing threshold [95]. The MQWs usually consist of GaAs/AlGaAs and strained InGaAs/AlGaAs, whereas the latter is usually preferred for high-speed applications for several reasons. The ternary alloy InGaAs improves the optical gain and the differential gain over those obtained with GaAs [12,13]. In addition, the indium composition lowers the effective bandgap and lessens the transparency current density in VCSELs [96].

For an improved optical gain with emphasis on high-speed characteristics, the inclusion of three to five MQWs inside the active region is preferable for enhancement of the differential gain within the critical thickness limitations [97]. In the meantime, the two-pole intrinsic responses are affected by current-induced self-heating, which leads to excessive damping and the intrinsic relaxation oscillation frequency. The resonance frequency (f_{R}) relates to the carrier interactions in the active region. The quantity of the carriers is transported through the SCHs and reaches the MQWs, and a proportion of them escape from the MQWs, causing a decrease in the differential gain. Efficient and modern high-speed VCSELs are tailored with large D-factors and reasonably low K-factors. In other words, high modulation bandwidths at low current injections emit moderate optical output powers.

4.3. Temperature Insensitive Design

Miniature-sized microcavities give VCSELs appealing potential for providing ultra-fast modulation bandwidths through the shrinkage of the device sizes. However, smaller cavities make VCSELs more susceptible to thermal-related effects, such as thermal-induced non-linear gain and self-heating [98], and an increase in the operating temperature is likely to cause an exacerbation of the device performance. Thermal-related non-linear effects in the laser gain may be caused by optical injection, optical feedback, current modulation, spectral hole burning, and mutual coupling in the optical cavity [14]. These issues negatively impair the performance of VCSELs and may result in further increases in the junction temperatures in the optical cavities. Eventually, this leads to declines in the differential gain, decreases in the device operating current ranges, reduced slope efficiencies, shorter lifetime, and significantly negative impacts on their large-signal performance.

One of the commonly applied techniques for enhancing high-temperature performance is the introduction of larger gain-to-cavity detunings. Cheng et al. incorporated an optimized large gain-to-cavity detuning and demonstrated temperature-insensitive 25.78 Gb/s VCSELs ready for 100GBASE-SR4 operation [23]. Additionally, the indium-induced compressive strain of the InGaAs QWs active region causes band splitting at the edges of the valence band, which benefits VCSEL operation at higher temperatures.

Consequently, it is vital to alleviate the current-induced temperature increases in the design process of high-speed, high-efficiency VCSELs, including but not limited to the lowering of the differential resistances, optical absorptions, thermal impedances, thermal conductivities, and non-radiative recombination rates. The use of binary semiconductors, such as AlAs, to supersede the conventional ternary AlGaAs may facilitate the spreading of the heat energy generated from the active region due to its better thermal conductivity [11].

Apart from enhancing the thermal instability capabilities of VCSELs through optimizations of the epitaxial layer and structural design, some modulation formats may be more resistant to harsh working environments. DMT also has proven capabilities for providing a more temperature-insensitive transmission channel [49]. Peng et al. demonstrated and argued that DMT has better transmission capabilities at an elevated temperature of 85 °C, as shown in Figure 12 [49].

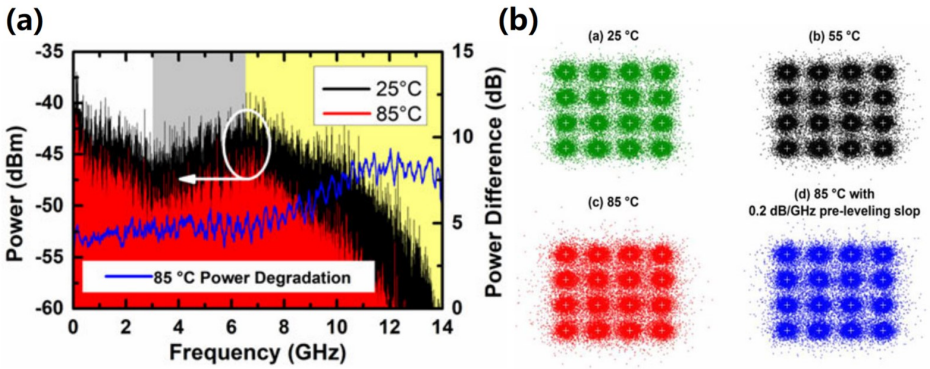

Figure 12. (**a**) The power spectrum of a VCSEL under 16-QAM-DMT at RT and 85 °C and (**b**) the constellation plots at RT, 55, and 85 °C; reprinted with permission from [49], Copyright © 2018 IEEE.

4.4. Characteristics of Modern High-Speed 850 nm VCSELs

Modern high-speed VCSELs usually consist of most of the design features described in this manuscript to exemplify a high-speed modulation bandwidth while providing sufficient optical outputs. In 2021, Yang et al. successfully fabricated and demonstrated a high-speed VCSEL for next-generation optical interconnects with two $Al_{0.98}Ga_{0.02}As$ oxidation layers for mode control and four $Al_{0.96}Ga_{0.04}As$ oxide layers for mesa capacitance reduction, as illustrated in Figure 13 [65]. The resonance peak is slightly damped with an optimized RC damping to ensure a flat E-O S_{21} response with a 3 dB bandwidth of ~30 GHz.

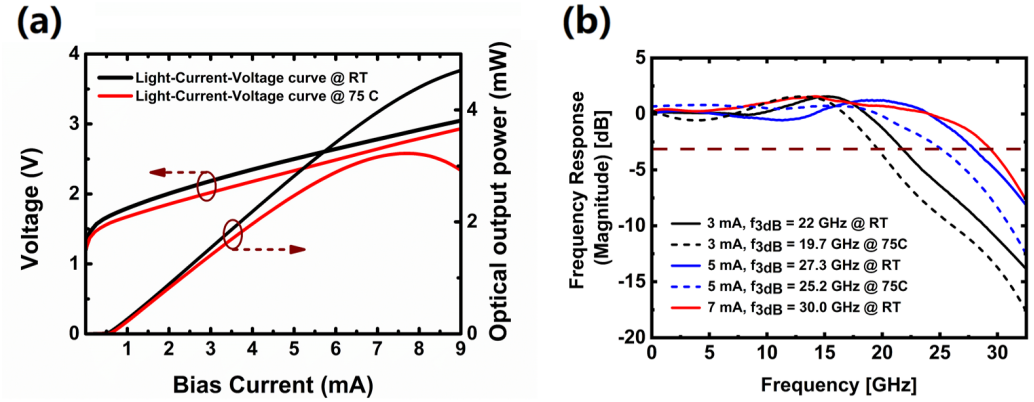

Figure 13. (**a**) The L-I-V and (**b**) microwave characteristics at RT and 75 °C for the VCSEL fabricated by Yang et al.; reprinted with permission from [65], Copyright © 2021 IEEE.

4.5. Small-Signal Modeling

In addition to the photon relaxation oscillations that influence VCSELs f_R, the parasitic damping effect due to the parasitic circuit elements inside the device has to be carefully designed for the sake of fast responses. The parasitic elements can be modeled as RLC circuits and depend on the device geometries, semiconductor structures, and fabrication processes. Figure 11 depicts an equivalent circuit of an oxide-confined VCSEL with the circuit components labeled on the schematic cross-sectional view in Figure 2. The small-signal circuit model portrays the microwave performance of VCSELs [21,93,99–105]. A VCSEL is biased with a current bias, I_{tot}, and the pumping current flowing through the intrinsic active-region laser junction is denoted as I_a. The forward operation in the laser junction diode is represented by the junction resistance, R_j, and the forward-biased diode junction capacitance is represented by C_j, where C_j mainly consists of the diffusion capacitance, C_{diff}, resulting from the minority carriers inside the active region, which primarily limit the modulation speed of VCSELs. The capacitances attributed to the oxidized regions of the oxidation layers and the intrinsic region below can be characterized by C_a. The mirror resistance, R_m, includes the resistances from both DBRs (sum of R_{m_p} and R_{m_n}). R_{sheet} represents the sheet resistance in the n-contact layer, and R_{cont} is the combined contact resistance for both contacts. These resistances can be simplified to account for only R_m, as it is usually much greater than the other two resistors (R_{sheet} and R_{cont}).

The resistor R_p accounts for the pad loss between the device's co-planar waveguide pads and the dielectric layer; since its value is relatively small, it is often omitted in some other small-signal models. The shunt capacitance C_p represents the pad's parasitic capacitance and varies in the range of a few tens to hundreds of fF depending on the design of the layout and the material between the source and ground, as discussed in Section 4.8.3.

Precise modeling of the electrical circuit elements in devices is essential for optimizing high-speed VCSELs. The scattering parameter $S_{11}(f)$ of the microwave reflection coefficient measured by a VNA can be used to predict the circuit elements.

4.6. D-Factor

The D-factor (also known as the modulation current efficiency factor (MCEF)) is the relation between f_R and $\sqrt{I - I_{th}}$, which is the square root of the differences between the bias current, I, and I_{th}. Therefore, D-factor = $f_R / \sqrt{I - I_{th}}$, and it is a notable figure of merit for high-speed VCSELs. The equation of f_R with respect to the D-factor is as follows:

$$f_R = D \cdot \sqrt{I - I_{th}} = \frac{1}{2\pi} \sqrt{\frac{\eta_i \Gamma v_g}{q V_a} \frac{a'}{\chi}} \tag{4}$$

where:

v_g = the group velocity of the light

a' = the material gain
q = the elementary electric charge
η_i = the internal quantum efficiency
Γ = the optical confinement factor in the active region
V_a = the volume of the active region (dependent on the oxide aperture size)
χ = the carrier transport factor indicating the speed of the carrier flowing from the confinement layer to the quantum well.

As shown in Equation (4), the D-factor is the correlated slope of f_R and $\sqrt{I - I_{th}}$, and it characterizes the conversion efficiency of E-O modulation. It was assumed that (i.) the changes in the rate of the injection carriers are equal to the emission rate of the photons and (ii.) there is no extra spontaneous mode coupling into the stimulated mode while the VCSELs operate above I_{th}. Equation (4) can be rewritten as:

$$f_R = \frac{1}{2\pi}\sqrt{\frac{v_g a'}{qV_a}\eta_i(I - I_{th})} \propto \frac{1}{2\pi}\sqrt{\frac{a'N_{th}}{a_{th}} \cdot \frac{1}{\tau_{rec}\tau_p}\left(\frac{I}{I_{th}} - 1\right)} \quad (5)$$

where:

N_{th} = the carrier density in the cavity
a_{th} = the material gain at the lasing threshold
τ_{rec} = the recombination carrier lifetime
τ_p = the photon lifetime.

Larger D-factors are generally preferred for the high-speed operation of VCSEL devices. Figure 14 shows the D-factor extracted at 11.49 GHz/$\sqrt{mA}$ for the high-speed VCSEL reported by Yang et al. [65]. This value is among the best reported to date, which is credited to the smaller-sized cavity [106,107].

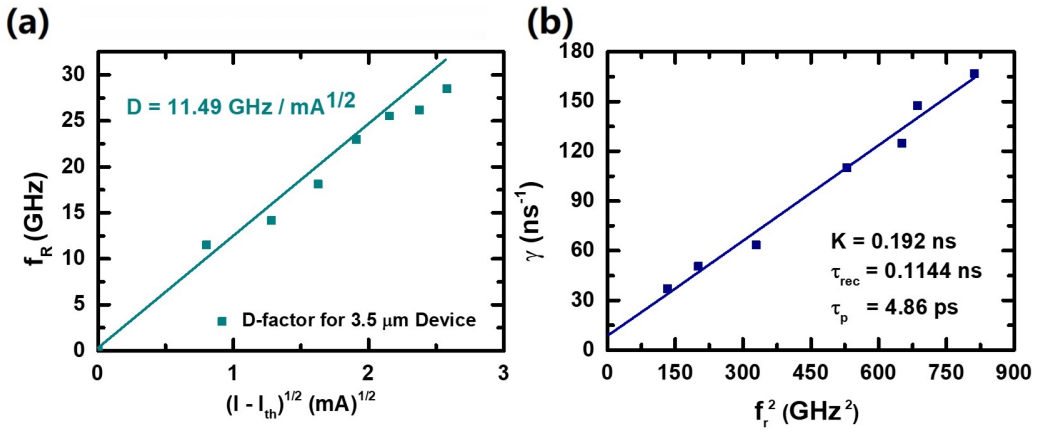

Figure 14. The extracted RT (**a**) D-factor and (**b**) K-factor of Yang et al.'s VCSEL from Figure 13 [65].

4.7. K-Factor

The K-factor can quantify the damping rate of VCSELs.

$$\gamma = Kf_R^2 + \gamma_0 \quad (6)$$

where:

K = $4\pi^2(\tau_p + (\varepsilon\chi/v_g a'))$
ε = the gain compression coefficient
γ_0 = the damping factor offset, which is inversely proportional to τ_{rec}.

The maximum optical modulation response $f_{3dB\text{-}max}$ of a VCSEL has a correlation to the enhancement of f_R, where a larger value of f_R could effectively producean extended $f_{3dB\text{-}max}$. VCSELs have a relatively fast radiative recombination lifetime because of the strengthening effect of the E-O conversion efficiency, which is due to the Purcell effect.

Equation (5) shows that f_R can be extended, thus achieving faster τ_{rec} and reducing lasing threshold in the VCSEL microcavity, which can be realized by using a small cavity length and tiny oxide aperture sizes [103,108]. In general, lower K-factors would be preferred for the high-speed VCSELs for reducing damping and thus higher bandwidths. The K-factor is partially dependent on the D-factor due to the linear relation between f_{3dB} and f_R at low currents.

4.8. Extrinsic Parasitic Optimizations

The maximum modulation response of VCSELs can be determined by the ratio between f_R and the damping constant. RC damping is one of the key limiting factors of the VCSEL modulation responses. Consequently, reduced damping is radical for the enhancement of the maximum 3 dB modulation response frequencies, but may lead to a strong resonance peak at the f_R of VCSELs. Crucially, it is important to emphasize that the magnitude and the frequency of the peaking in the modulation response cause overshooting and ringing, which further degrade the large-signal performance of VCSELs. The damping rate can be quantified by the K-factor, which is affected by the photon lifetime in the VCSEL cavities.

With the equivalent small-signal model illustrated in Figure 11 in mind, the extrinsic parasitic elements can be extracted and investigated. The extrinsic parasitic elements can be represented by resistors and capacitors in the small-signal model. These parasitic elements literally form an RC low-pass filter, which can be represented by a single-pole transfer function, Equation (3) [14].

The resistance inside the device is mainly contributed by junction resistance and the n-type/p-type DBRs' resistance. In order to simultaneously lower the mirror resistance with the lowest free-carrier absorption, modulation doping [109], delta doping [110], and graded interfaces [111] are often used in the design methodology for VCSELs. The excessive capacitance inside the device would be inimical to the overall optical modulation bandwidth of VCSELs, as mentioned before. Using graded or narrow SCH could potentially decrease the diffusion capacitance and enhance the speed of VCSELs [112]. The mesa capacitance can be reduced by using a thicker oxidized layer and multiple deep oxidation layers [113–115]. This can be achieved through the incorporation of multiple high-aluminum-content AlGaAs layers of different compositions for the formation of multiple oxidation confinement layers.

The core idea of the enhancement of the VCSEL E-O modulation bandwidth is the extension of the intrinsic modulation rate and the lowering of the extrinsic parasitic damping effects. Since the attempts of Jewell et al. and Coldren et al. to minimize the VCSEL and lower the threshold of lasing [4,5], the reduction in the device sizes and cavity lengths and the lowering of the parasitic effects have become the core of extending the modulation bandwidth of VCSELs.

4.8.1. Epilayer Optimizations

The differential resistances of VCSELs are mainly contributed by R_m. As the top p-type DBR mirrors have much lower hole mobilities, R_{m_p} occupies a significant portion of the total R_m. The top p-type mirrors are usually more heavily doped to decrease the device's differential resistance. In the meantime, higher doping levels may lead to increased free-carrier absorption due to the p-type background doping, which increases the lasing threshold and degrades the output efficiency. Graded layers and delta doping in the heterointerfaces eliminate the energy-band discontinuities and allow lower interface resistivity. Additionally, using accurately selective doping levels on different layers according to the nodes' and antinodes' distribution reduces excessive absorption while maintaining low mirror resistivity.

Techniques such as the introduction of multi-oxide deep oxidation layers significantly reduce the parasitic capacitance and increase the overall E-O modulation bandwidth of VCSELs [113,114]. In addition, there have been reports on the use of etching techniques for

the formation of an oxide-relief confinement layer and to provide a further reduction in the mesa parasitic capacitance [81,86].

4.8.2. Layout Optimizations

Optimized co-planar waveguide designs allow further reductions of the RC parasitic elements [99,101]. A smaller mesa size reduces the mesa capacitance and extends the modulation bandwidth. A smaller oxidation aperture size shrinks the optical volume and the lasing threshold, but might increase the device's differential resistance. In addition, using passivation materials with low dielectric permittivities (ε_r) may further reduce the pad parasitic capacitance and enhance the high-speed performance [16,18]. One of the limiting factors for high-frequency operation comes from the parasitic capacitance of contact bonding pads, which is proportional to ε_R of the passivation material. Adopting low-k material can extend the cut-off frequency and further improve the impact of the RC low-pass behavior on the optical modulation response [65,100]. Likewise, removing the area of the layer underneath the contact pads can also reduce the capacitance when fabricating high-impedance co-planar transmission lines [105].

4.8.3. Passivation Materials

The common choices of passivation for VCSELs with the functionalities of protecting sidewall and insulation are summarized in Table 1. Polyimide and BCB have lower ε_r, which may further reduce the pad parasitic capacitance and enhance the high-speed performance of VCSELs [16,18].

Table 1. Selection of passivation materials.

	SiN	**Polyimide**	**BCB**
Dielectric constant (ε_R)	7.5 [15]	3.4 [17]	2.5 [19]
First applied on VCSEL	1994 [15]	1997 [16]	2005 [18]
Common deposition method	CVD	Spin coating	Spin coating
Pad capacitance	Large $\sim$ pF	Small $\leq$ 100 fF	Minimal $\leq$ 100 fF
Step coverage	Excellent	Good	Good
Planarization effect	Mediocre	Excellent	Excellent
Cost	Cheap	Moderate	Expensive

4.8.4. Impurity-Induced Disordering

As mentioned in Section 3.2, FM and SM VCSELs are usually tormented with higher differential resistances, early thermal roll-overs resulting in lower roll-over currents, reduced optical output powers, and reduced modulation bandwidths due to the increased differential resistances and operating currents. Some processing techniques have been applied to VCSELs with the aim of tackling the differential resistance and thermal resistance issues that plague small-aperture oxide-confined VCSELs through the introduction of IID technology [71,79–85,89]. IID VCSELs show the characteristics of a high speed, outstanding efficiency, highly single mode, lower differential resistance, and relatively higher optical power [71,81,82,84,85]. Therefore, IID VCSELs with FM or SM characteristics show excellent mid- to long-range transmission capabilities [71,83,85].

The IID techniques introduce intermixing and impurities in the top DBR regions outside of the emitting window, as shown in the inset SEM image in Figure 15a, as they increase the DBR mirror losses and free carrier absorption. The IID process results in a mode selection mechanism that significantly reduces the emission power of the higher-order modes. The presence of a heavily Zn-doped layer near the P-contact layers via IID results in a significant decrease in contact resistance, as illustrated in Figure 15b [84].

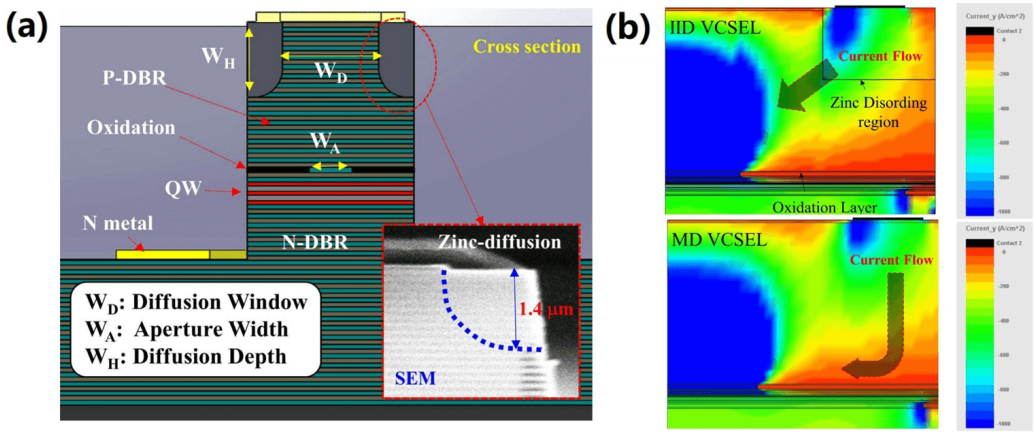

Figure 15. (**a**) A cross-sectional view and an SEM image (inset figure) of an IID VCSEL; (**b**) simulation results of the threshold current distributions of the IID VCSEL and a conventional VCSEL when operating at RT; reprinted with permission from [84], Copyright © 2020 IEEE.

5. Historical Review of Modern 850 nm VCSELs and Features of Next-Generation High-Speed VCSELs

After 44 years of development, remarkable progress has been made on the development of VCSELs, and many researchers have demonstrated ultra-fast VCSELs with modulation bandwidths of up to 30 GHz [22,61–65,116]. Some of the selected works on 850 nm VCSELs are shown in Figure 16 and Table 2.

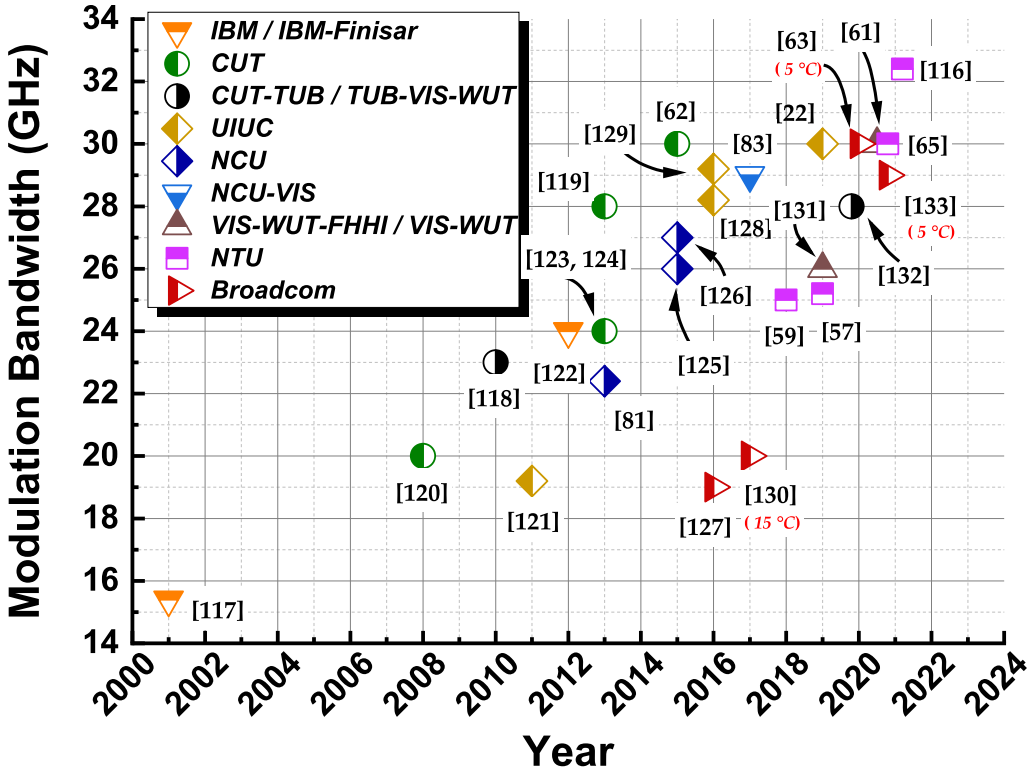

Figure 16. Selected results for 3 dB bandwidths of 850 nm VCSELs at RT (unless stated otherwise) [22,57,59,61–63,65,81,83,116–133].

Table 2. Selected results of 3 dB bandwidths for 850 nm VCSELs with NRZ, PAM-4, DMT, OFDM, and GFDM modulation formats at RT (unless stated otherwise).

Group	Data Rate (Gb/s)	Modulation Format	3 dB Bandwidth (GHz)	Temperature (°C)	Distance (m)	Reference	Year	Bare Chip/ Packaged
CUT	25	NRZ	20	25	BtB	[120]	2008	Bare chip
CUT	47	NRZ	28	25	BtB	[119]	2013	Bare chip
CUT	60 (30 GBd)	PAM-4	24	25	BtB	[123]	2013	Bare chip
CUT	57	NRZ	24	25	BtB	[124]	2013	Bare chip
CUT	50	NRZ	30	25	BtB	[62]	2015	Bare chip
UIUC	40	NRZ	19.2	25	BtB	[121]	2011	Bare chip
UIUC	50	NRZ	28.2	25	BtB	[128]	2016	Bare chip
UIUC	57	NRZ	29.2	25	BtB	[129]	2016	Bare chip
UIUC	28	NRZ	17.3	25	1000	[70]	2019	Bare chip
UIUC	50	NRZ	30.03	25	100	[22]	2019	Bare chip
UIUC	44	NRZ	N/A	25	500	[134]	2021	Bare chip
UIUC	64 (32 GBd)	PAM-4	N/A	25	500	[134]	2021	Bare chip
CUT-TUB	32	NRZ	20	25	50	[135]	2009	Bare Chip
CUT-TUB	40	NRZ	23	25	BtB	[118]	2010	Bare chip
TUB	40/36	NRZ	N/A	25	BtB/200	[136]	2013	Bare chip
TUB-VIS-WUT	120 (60 GBd)	PAM-4	28	25	BtB	[132]	2019	Bare chip
NCU	40	NRZ	22.4	25	BtB	[81]	2013	Bare chip
NCU	41	NRZ	26	25	BtB & 100	[125]	2015	Bare chip
NCU	41	NRZ	27	25	BtB & 100	[126]	2015	Bare chip
NCU-VIS	54	NRZ	29	25	BtB & 1000	[83]	2017	Bare chip
IBM	20	NRZ	15.4	25	BtB	[117]	2001	Packaged
IBM-Finisar	55	NRZ	24	25	BtB	[122]	2012	Packaged
WUT-VIS	54	NRZ	N/A	25	2200	[137]	2015	Packaged
VIS-WUT-FHHI	56	NRZ	22 & 26	25	BtB	[131]	2019	Packaged (56 Gb/s w/ 22 GHz VCSEL)
VIS-WUT	80	NRZ	30	25	BtB	[61]	2020	Packaged
GIT-VIS-WUT	168 (84 GBd)	PAM-4	28	25	BtB	[51]	2020	Packaged
VIS-WUT	50	NRZ	30	25	BtB	[64]	2021	Packaged
VIS-WUT	106 (53 GBd)	PAM-4	30	25	BtB	[64]	2021	Packaged
VIS-WUT-FHHI	224	4-QAM DMT	~26.8	25	BtB	[54]	2021	Packaged
Finisar	45 (22.5 GBd)	PAM-4	N/A	25	BtB	[138]	2016	Packaged
Finisar	50 (25 GBd)	PAM-4	20	25	BtB & 200	[139]	2015	Packaged
Broadcom	54 (27 GBd)	PAM-4	19	25	BtB	[127]	2016	Bare Chip
Broadcom	53.125 (26.5625 GBd)	PAM-4	20 (15 °C)	15	200	[130]	2017	Bare Chip
Broadcom	106.25 (53.125 GBd)	PAM-4	30 (5 °C)	25	75	[63]	2020	Bare Chip
Broadcom	106.25 (53.125 GBd)	PAM-4	29 (5 °C)	25	100	[133]	2021	Bare Chip
NTU	80	16-QAM OFDM	21.5	25	100	[55]	2017	Bare chip
NTU	50	NRZ	25	25	BtB	[59]	2018	Bare chip
NTU	96	16-QAM OFDM	22.1	25	100	[56]	2018	Bare chip
NTU	64 (32 GBd)	PAM-4	18.9	25	BtB	[140]	2018	Bare chip
NTU	54	NRZ	N/A	25	BtB	[60]	2019	Bare chip
NTU	140	16-QAM OFDM	25.2	25	BtB	[57]	2019	Bare chip
NTU	40	NRZ	26.6	25	500	[71]	2020	Bare chip
NTU	61	NRZ	20.7	25	BtB	[58]	2020	Bare chip
NTU	82 (42 GBd)	PAM-4	17.7	25	BtB	[50]	2020	Bare chip
NTU	132	16-QAM OFDM	17.7	25	BtB	[50]	2020	Bare chip
NTU	102 (51 GBd)	PAM-4	20.7	25	BtB	[58]	2020	Bare chip
NTU	124	32-QAM GFDM	20.7	25	BtB	[58]	2020	Bare chip
NTU-Corning	53	NRZ	N/A	25	100	[85]	2021	Bare chip
NTU	N/A	N/A	30	25	BtB	[65]	2021	Bare chip
NTU	N/A	N/A	32.4	25	BtB	[116]	2021	Bare chip

Note: This table summarizes the maximum data rates and 3-dB bandwidths at RT (unless stated otherwise) reported in these manuscripts. The maximum data rates and the 3-dB bandwidths might be observed at different injection currents.

5.1. Benchmarking of the State-of-the-Art 850 nm VCSELs at RT

In 2001, IBM Inc. demonstrated an oxide-confined VCSEL with a 15.4 GHz modulation response and successfully achieved 20 Gb/s OOK transmission over 2 km using an integrated SiGe VCSEL driver [117]. In 2010, Larsson's group at Chalmers University of Technology (CUT) and Bimberg's group at TU Berlin (TUB) reported a VCSEL with a record 23 GHz modulation bandwidth by implementing a multi-oxide layer for decreased parasitic capacitance [113,114] and achieved a data rate for back-to-back transmission of up to

40 Gb/s without forward error correction (FEC) [118]. By shrinking the oxide aperture and using multiple oxidized layers, Larsson's group demonstrated VCSELs with a modulation bandwidth of up to 28 GHz and 47 Gb/s error-free transmission with NRZ in 2013 [119]. In the same year, Shi's group from National Central University, Taiwan (NCU) used impurity-induced disordering, i.e., Zn diffusion [141], and oxide-relief processes in 850 nm VCSEL, and the fabricated devices had a 3 dB modulation bandwidth of 22.4 GHz and up to 40 Gb/s NRZ transmission [81]. In 2015, Larsson's group reported a record highly efficient 30 GHz VCSEL when biased at a relatively low current of 4.1 mA [62]. In 2019, Huang et al. demonstrated 54 Gb/s error-free BtB transmission with a 4.23 μm oxide aperture VCSEL device [60]. In 2021, Yang et al. reported a 30 GHz VCSEL with 2 $Al_{0.98}Ga_{0.02}As$ oxidation layers for mode control and 4 $Al_{0.96}Ga_{0.04}As$ oxide layers for the reduction of mesa capacitance [65]. In October 2021, Yang et al. fabricated and demonstrated an ultra-fast 850 nm VCSEL with a modulation bandwidth of 32.4 GHz [116].

5.2. Features of Next-Generation VCSELs

Valuable progress has been made in the development of devices and advanced modulation formats to enable high modulation responses and energy-efficient and rapid data transmission using VCSELs in the last few decades. Significant achievements have been made in the improvement of 850 nm VCSELs' modulation bandwidths, and the fastest reported 3 dB modulation bandwidth to date is ∼30 GHz [22,61–65,116]. On the other hand, more work has to be done to standardize and commercialize these high-speed 850 nm VCSELs in commercial transceivers to enable the future 800 GbE and 1.6 TbE Ethernets.

The current common Ethernet standard is 100GBASE-SR4, which is comprised of four 25.78 Gb/s VCSEL channels. However, it is inefficient to use optical lanes with 25 Gb/s to drive the current 400 GbE and the future 800 GbE and 1.6 TbE haul rates. Hence, it has become utterly essential to develop individual VCSEL chips that carry data rates that are >100 Gb/s, and the datacom industry has been developing 56 GBd VCSELs using PAM-4 to enable a data rate of 112 Gb/s. The IEEE and the Organisation internationale de la Francophonie (OIF) have developed 106–112 Gb/s per lane in IEEE Std. P802.3ck and CEI-112 G for the 400 GbE system [47,48]. VCSEL market leaders Broadcom and VIS have developed commercial 112 Gb/s (56 GBd) VCSEL chips for optical interface transceivers. However, they are still in the preliminary stage, and the standardization of the optical interface is still underway [142,143].

The multi-level modulation format PAM-4 is highly vulnerable to intersymbol interference (ISI), thus placing great importance on the dynamic performance of VCSELs, such as a high bandwidth at low current, highly damped S_{21} response, and low intrinsic noise. In addition, noise-contributing factors in fiber transmissions, such as dispersion effects, RIN, and power losses, should be minimized [144]. Reduced channel noise remarkably reduces the reliance on DSP for pre-compensating the optical channel noise [72]. TDECQ (Transmitter and Dispersion Eye Closure Quaternary) was introduced to calculate the penalty for transmitters that have unequal sub-eyes in a significantly easier way [33].

In the meantime, the investigation and development of energy-efficient VCSEL chips are becoming increasingly important, as laser-driver IC designers generally prefer highly efficient VCSELs with large modulation bandwidths at low operating currents to reduce the requirements for the compensating circuitries. Researchers have been working on improving the efficiencies of VCSELs [145–147]. In 2013, Moser et al. demonstrated energy-efficient VCSELs with a dissipated power per bit as low as 56 fJ/bit [146]. While efficient VCSELs with high bit energies are highly desired, improved optical modulation amplitudes (OMAs) and reduced noise may improve their transmission quality [147].

6. Conclusions

This manuscript discussed and reviewed the recent developments of high-speed 850 nm VCSELs and their commonly used modulation formats. We also discussed the design and optimization of high-speed 850 nm VCSELs from different perspectives, in-

cluding device design, mode control, and temperature insensitivity. Starting from the laser transfer functions and small-signal models, we explained the contributing factors of the intrinsic and extrinsic responses of VCSELs and the critical considerations for the design of the active regions and RC parasitic optimization. Then, we discussed the mode behavior in VCSELs and their influences on large-signal modulation. Lastly, we summarized a historical review of modern high-speed 850 nm VCSELs and the key considerations for future next-generation VCSELs.

We believe that the miniature size, high efficiency, high speed, narrow spectral width, flat microwave response, and capabilities of achieving high modulation bandwidth at small current densities are features of modern VCSELs that are not to be neglected. We cannot emphasize the importance of these features in the consideration and design of next-generation high-speed 850 nm VCSELs for interconnects enough.

Author Contributions: Conceptualization, H.-T.C. and C.-H.W.; investigation, H.-T.C., Y.-C.Y. and T.-H.L.; data curation, H.-T.C., Y.-C.Y. and T.-H.L.; writing—original draft preparation, H.-T.C., Y.-C.Y. and C.-H.W.; writing—review and editing, H.-T.C. and C.-H.W.; funding acquisition, C.-H.W. All authors have read and agreed to the published version of the manuscript.

Funding: This research was funded by the Ministry of Science and Technology, Taiwan, grant numbers MOST 108-2823-8-002-004, MOST 108-2218-E-992-302, MOST 108-2823-002-004, MOST 109-2221-E-002-183-MY2, MOST 109-2224-E-992-001, and MOST 109-2622-E-002-020-CC2, and by National Taiwan University, grant numbers 108L7819, 109L2033-49, 109L7819, and 110L2033-49.

Data Availability Statement: All relevant data are available from the authors upon reasonable request.

Acknowledgments: The authors acknowledge the grants and support from the Ministry of Science and Technology, Taiwan (R.O.C.) and National Taiwan University, Taiwan (R.O.C.). The authors would like to thank all colleagues and members of the Integrated Optoelectronic Device Group (IOED) of National Taiwan University who contributed to our research on high-speed VCSELs and other optoelectronic devices.

Conflicts of Interest: The authors declare no conflict of interest.

References

1. Iga, K.; Kambayashi, T.; Kitahara, C. Surface-emitting GaInAsP/InP laser (I). In Proceedings of the 25th Joint Conference on Applied Physics, Tokyo, Japan, 27 March 1978; p. 63.
2. Soda, H.; Iga, K.; Kitahara, C.; Suematsu, Y. GaInAsP/InP Surface Emitting Injection Lasers. *Jpn. J. Appl. Phys.* **1979**, *18*, 2329–2330. [CrossRef]
3. Iga, K.; Koyama, F.; Kinoshita, S. Surface emitting semiconductor lasers. *IEEE J. Quantum Electron.* **1988**, *24*, 1845–1855. [CrossRef]
4. Jewell, J.L.; Huang, K.F.; Tai, K.; Lee, Y.H.; Fischer, R.J.; McCall, S.L.; Cho, A.Y. Vertical cavity single quantum well laser. *Appl. Phys. Lett.* **1989**, *55*, 424–426. [CrossRef]
5. Corzine, S.; Geels, R.; Scott, J.; Yan, R.H.; Coldren, L. Design of Fabry-Perot surface-emitting lasers with a periodic gain structure. *IEEE J. Quantum Electron.* **1989**, *25*, 1513–1524. [CrossRef]
6. Jewell, J.; Scherer, A.; McCall, S.; Lee, Y.H.; Walker, S.; Harbison, J.; Florez, L. Low-Threshold Electrically Pumps Vertical-Cavity Surface-Emitting Microlasers. *Electron. Lett.* **1989**, *25*, 1123–1124. [CrossRef]
7. Optical Transceivers for Datacom & Telecom Market 2021 Report. Available online: https://www.i-micronews.com/products/optical-transceivers-for-datacom-telecom-market-2021/?utm_source=PR&utm_medium=email&utm_campaign=PR_OPTICAL_TRANSCEIVERS_FOR_DATACOM_AND_TELECOM_YOLEGROUP_July2021 (accessed on 5 January 2022).
8. Dallesasse, J.M.; Gavrilovic, P.; Holonyak, N.; Kaliski, R.W.; Nam, D.W.; Vesely, E.J.; Burnham, R.D. Stability of AlAs in $Al_xGa_{1-x}As$-AlAs-GaAs quantum well heterostructures. *Appl. Phys. Lett.* **1990**, *56*, 2436–2438. [CrossRef]
9. Huffaker, D.L.; Deppe, D.G.; Kumar, K.; Rogers, T.J. Native-oxide defined ring contact for low threshold vertical-cavity lasers. *Appl. Phys. Lett.* **1994**, *65*, 97–99. [CrossRef]
10. Dallesasse, J.M.; Deppe, D.G. III–V Oxidation: Discoveries and Applications in Vertical-Cavity Surface-Emitting Lasers. *Proc. IEEE* **2013**, *101*, 2234–2242. [CrossRef]
11. Afromowitz, M.A. Thermal conductivity of $Ga_{1-x}Al_xAs$ alloys. *J. Appl. Phys.* **1973**, *44*, 1292–1294. [CrossRef]
12. Corzine, S.W.; Yan, R.H.; Coldren, L.A. Theoretical gain in strained InGaAs/AlGaAs quantum wells including valence-band mixing effects. *Appl. Phys. Lett.* **1990**, *57*, 2835–2837. [CrossRef]

13. Aggerstam, T.; von Wurtemberg, R.M.; Runnstrom, C.; Choumas, E. Large aperture 850 nm oxide-confined VCSELs for 10Gb/s data communication. In *Vertical-Cavity Surface-Emitting Lasers VI*; Lei, C., Kilcoyne, S.P., Eds.; International Society for Optics and Photonics, SPIE: Bellingham, WA, USA, 2002; Volume 4649, pp. 19–24. [CrossRef]
14. Coldren, L.; Corzine, S. *Diode Lasers and Photonic Integrated Circuits*; Wiley: Hoboken, NJ, USA, 1995.
15. Young, D.; Kapila, A.; Scott, J.; Malhotra, V.; Coldren, L. Reduced threshold vertical-cavity surface-emitting lasers. *Electron. Lett.* **1994**, *30*, 233–235. [CrossRef]
16. Lear, K.; Hietala, V.; Hou, H.; Banas, J.; Hammons, B.; Zolper, J.; Kilcoyne, S. Small and large signal modulation of 850 nm oxide-confined verticai-cavity surface-emitting lasers. In Proceedings of the CLEO'97, Summaries of Papers Presented at the Conference on Lasers and Electro-Optics, Baltimore, MD, USA, 18–23 May 1997; Volume 11, pp. 193–194. [CrossRef]
17. AL-Omari, A.N.; Lear, K.L. Dielectric characteristics of spin-coated dielectric films using on-wafer parallel-plate capacitors at microwave frequencies. *IEEE Trans. Dielectr. Electr. Insul.* **2005**, *12*, 1151–1161. [CrossRef]
18. Tanigawa, T.; Onishi, T.; Nagai, S.; Ueda, T. High-speed 850 nm AlGaAs/GaAs vertical cavity surface emitting laser with low parasitic capacitance fabricated using BCB planarization technique. In Proceedings of the CLEO, Conference on Lasers and Electro-Optics, Baltimore, MD, USA, 22–27 May 2005; Volume 2, pp. 1381–1383. [CrossRef]
19. The Dow Chemical Company. Advanced Packaging Polymers Product Selection Guide. Available online: https://www.microresist.de/en/?jet_download=4823 (accessed on 5 January 2022).
20. Jiang, W.J.; Chen, L.C.; Wu, M.C.; Yu, H.C.; Yang, H.P.; Sung, C.P.; Chi, J.Y.; Huang, C.Y.; Wu, Y.T. A new process to improve the performance of 850 nm wavelength GaAs VCSELs. *Solid-State Electron.* **2002**, *46*, 2287–2289. [CrossRef]
21. Wang, C.Y.; Liu, M.; Feng, M.; Holonyak, N. Microwave extraction method of radiative recombination and photon lifetimes up to 85 °C on 50 Gb/s oxide-vertical cavity surface emitting laser. *J. Appl. Phys.* **2016**, *120*, 223103. [CrossRef]
22. Wang, H.L.; Fu, W.; Qiu, J.; Feng, M. 850 nm VCSELs for 50 Gb/s NRZ Error-Free Transmission over 100-meter OM4 and up to 115 °C Operation. In Proceedings of the 2019 Optical Fiber Communication Conference (OFC), San Diego, CA, USA, 3–7 March 2019; p. W3A.1. [CrossRef]
23. Cheng, H.T.; Yang, Y.C.; Wu, C.H. High thermal stability of 850 nm VCSELs with enhanced mask margin up to 85 °C for 100G-SR4 Operation. In Proceedings of the 2021 30th Wireless and Optical Communications Conference (WOCC), Taipei, Taiwan, 7–8 October 2021; pp. 49–53. [CrossRef]
24. Iga, K.; Li, H. *Vertical-Cavity Surface-Emitting Laser Devices*; Springer: Berlin/Heidelberg, Germany, 2003. [CrossRef]
25. Dummer, M.; Johnson, K.; Rothwell, S.; Tatah, K.; Hibbs-Brenner, M. The role of VCSELs in 3D sensing and LiDAR. In *Optical Interconnects XXI*; Schröder, H., Chen, R.T., Eds.; International Society for Optics and Photonics, SPIE: Bellingham, WA, USA, 2021; Volume 11692, pp. 42–55. [CrossRef]
26. CommScope. Solutions for Multi Tenant Data Centers: HD Fiber. Available online: https://www.flickr.com/photos/48464290@N05/36135239403 (accessed on 5 January 2022).
27. Wu, H.; Fu, W.; Feng, M.; Deppe, D. 2.6 K VCSEL data link for cryogenic computing. *Appl. Phys. Lett.* **2021**, *119*, 041101. [CrossRef]
28. Vishay Intertechnology. New IRED- and VCSEL-Powered VCNL36821S and VCNL36826S Proximity Sensors Feature Power Consumption Down to 6 µA in 2.55 mm × 2.05 mm × 1.0 mm SMD Package for Consumer and Industrial Applications. Available online: https://www.flickr.com/photos/43093990@N05/49339783313 (accessed on 5 January 2022).
29. Jurvetson. Velodyne High-Def LIDAR Photo by Jurvetson. Available online: https://www.flickr.com/photos/44124348109@N01/4042817787 (accessed on 5 January 2022).
30. Velodyne Lidar. Velodyne's HDL-64E Lidar Sensor Looks Back on a Legendary Career. Available online: https://velodynelidar.com/products/hdl-64e (accessed on 5 January 2022).
31. IEEE Standard for Information Technology–Local and Metropolitan Area Networks–Part 3: CSMA/CD Access Method and Physical Layer Specifications–Media Access Control (MAC) Parameters, Physical Layer, and Management Parameters for 10 Gb/s Operation. *IEEE Std 802.3ae-2002 (Amendment to IEEE Std 802.3-2002).* 2002; pp. 1–544. Available online: https://ieeexplore.ieee.org/document/1040118 (accessed on 5 January 2022). [CrossRef]
32. IEEE Standard for Ethernet–Amendment 3: Physical Layer Specifications and Management Parameters for 40 Gb/s and 100 Gb/s Operation over Fiber Optic Cables. *IEEE Std 802.3bm-2015 (Amendment to IEEE Std 802.3-2012 as amended by IEEE Std 802.3bk-2013 and IEEE Std 802.3bj-2014).* 2015; pp. 1–172. Available online: https://standards.ieee.org/ieee/802.3bm/5657/ (accessed on 5 January 2022). [CrossRef]
33. IEEE Standard for Ethernet—Amendment 10: Media Access Control Parameters, Physical Layers, and Management Parameters for 200 Gb/s and 400 Gb/s Operation. *IEEE Std 802.3bs-2017 (Amendment to IEEE 802.3-2015 as amended by IEEE's 802.3bw-2015, 802.3by-2016, 802.3bq-2016, 802.3bp-2016, 802.3br-2016, 802.3bn-2016, 802.3bz-2016, 802.3bu-2016, 802.3bv-2017, and IEEE 802.3-2015/Cor1-2017).* 2017; pp. 1–372. Available online: https://ieeexplore.ieee.org/document/8207825 (accessed on 5 January 2022). [CrossRef]
34. IEEE Standard for Ethernet–Amendment 7: Physical Layer and Management Parameters for 400 Gb/s over Multimode Fiber. *IEEE Std 802.3cm-2020 (Amendment to IEEE Std 802.3-2018 as amended by IEEE Std 802.3cb-2018, IEEE Std 802.3bt-2018, IEEE Std 802.3cd-2018, IEEE Std 802.3cn-2019, IEEE Std 802.3cg-2019, and IEEE Std 802.3cq-2020).* 2020; pp. 1–72. Available online: https://ieeexplore.ieee.org/document/9052826 (accessed on 5 January 2022). [CrossRef]

35. Ethernet Alliance. The 2020 Ethernet Roadmap. Available online: https://ethernetalliance.org/wp-content/uploads/2020/03/EthernetRoadmap-2020-Side1-FINAL.pdf (accessed on 5 January 2022).
36. Sun, P.; Kretzschmar, H.; Dotiwalla, X.; Chouard, A.; Patnaik, V.; Tsui, P.; Guo, J.; Zhou, Y.; Chai, Y.; Caine, B.; et al. Scalability in perception for autonomous driving: Waymo open dataset. In Proceedings of the IEEE/CVF Conference on Computer Vision and Pattern Recognition, Seattle, WA, USA, 13–19 June 2020; pp. 2446–2454. [CrossRef]
37. SONY. Optical Disc Archive Generation 2. Available online: https://pro.sony/s3/cms-static-content/file/49/1237494482649.pdf (accessed on 5 January 2022).
38. Mukoyama, N.; Otoma, H.; Sakurai, J.; Ueki, N.; Nakayama, H. VCSEL Array-Based Light Exposure System for Laser Printing. In *Vertical-Cavity Surface-Emitting Lasers XII*; Lei, C., Guenter, J.K., Eds.; International Society for Optics and Photonics, SPIE: Bellingham, WA, USA, 2008; Volume 6908, pp. 146–156. [CrossRef]
39. Krinner, S.; Storz, S.; Kurpiers, P.; Magnard, P.; Heinsoo, J.; Keller, R.; Lütolf, J.; Eichler, C.; Wallraff, A. Engineering cryogenic setups for 100-qubit scale superconducting circuit systems. *EPJ Quantum Technol.* **2019**, *6*, 2. [CrossRef]
40. Cheng, H.T.; Wu, C.H.; Fu, W.; Wang, H.L.; Feng, M.; Wu, C.H. Cryogenic operation of a high speed 850 nm VCSEL with 40.1 GHz modulation bandwidth at 223 K. In Proceedings of the 2020 Opto-Electronics and Communications Conference (OECC), Taipei, Taiwan, 4–8 October 2020; pp. 1–3. [CrossRef]
41. Fu, W.; Wu, H.; Wu, D.; Feng, M.; Deppe, D. Cryogenic Oxide-VCSEL for PAM-4 Optical Data Transmission Over 50 Gb/s at 77 K. *IEEE Photonics Technol. Lett.* **2021**, *33*, 816–819. [CrossRef]
42. SFF Committee. INF-8074 SFP (Small Formfactor Pluggable) Tansceiver. Available online: https://members.snia.org/document/dl/26184 (accessed on 5 January 2022).
43. SFF Committee. SFF-8431 SFP+ 10 Gb/s and Low Speed Electrical Interface. Available online: https://members.snia.org/document/dl/25891 (accessed on 5 January 2022).
44. SFF Committee. SFF-8402 SFP+ 1X 28 Gb/s Pluggable Transceiver Solution (SFP28). Available online: https://members.snia.org/document/dl/25869 (accessed on 5 January 2022).
45. SFF Committee. SFF-8436 QSFP+ 4X 10 Gb/s Pluggable Transceiver. Available online: https://members.snia.org/document/dl/25896 (accessed on 5 January 2022).
46. SFF Committee. SFF-8665 QSFP+ 28 Gb/s 4X Pluggable Transceiver Solution (QSFP28). Available online: https://members.snia.org/document/dl/25963 (accessed on 5 January 2022).
47. Institute of Electrical and Electronics Engineers. IEEE 802.3 100 Gb/s, 200 Gb/s, and 400 Gb/s Electrical Interfaces Task Force. Available online: http://www.ieee802.org/3/ck/index.html (accessed on 5 January 2022).
48. Organisation internationale de la Francophonie. OIF CEI-112 G XSR, VSR, MR, and LR Working Group. Available online: https://www.oiforum.com/technical-work/current-work/ (accessed on 5 January 2022).
49. Peng, C.Y.; Tsai, C.T.; Wang, H.Y.; Wu, Y.C.; Shih, T.T.; Huang, J.J.; Kuo, H.C.; Cheng, W.H.; Lin, G.R.; Wu, C.H.W. High-Temperature Insensitivity of 50-Gb/s 16-QAM-DMT Transmission by Using the Temperature-Compensated Vertical-Cavity Surface-Emitting Lasers. *J. Light. Technol.* **2018**, *36*, 3332–3343. [CrossRef]
50. Huang, C.Y.; Wang, H.Y.; Peng, C.Y.; Tsai, C.T.; Wu, C.H.; Lin, G.R. Multimode VCSEL Enables 42-GBaud PAM-4 and 35-GBaud 16-QAM OFDM for 100-m OM5 MMF Data Link. *IEEE Access* **2020**, *8*, 36963–36973. [CrossRef]
51. Lavrencik, J.; Varughese, S.; Ledentsov, N.; Chorchos, Ł.; Ledentsov, N.N.; Ralph, S.E. 168Gbps PAM-4 Multimode Fiber Transmission through 50m using 28GHz 850nm Multimode VCSELs. In Proceedings of the Optical Fiber Communication Conference (OFC) 2020, San Diego, CA, USA, 8–12 March 2020; p. W1D.3. [CrossRef]
52. Zhong, K.; Zhou, X.; Gui, T.; Tao, L.; Gao, Y.; Chen, W.; Man, J.; Zeng, L.; Lau, A.P.T.; Lu, C. Experimental study of PAM-4, CAP-16, and DMT for 100 Gb/s Short Reach Optical Transmission Systems. *Opt. Express* **2015**, *23*, 1176–1189. [CrossRef]
53. Puerta, R.; Agustin, M.; Chorchos, Ł.; Toński, J.; Kropp, J.R.; Ledentsov, N.; Shchukin, V.; Ledentsov, N.; Henker, R.; Monroy, I.T.; et al. 107.5 Gb/s 850 nm multi- and single-mode VCSEL transmission over 10 and 100 m of multi-mode fiber. In Proceedings of the Optical Fiber Communication Conference Postdeadline Papers, Anaheim, CA, USA, 20–22 March 2016; p. Th5B.5. [CrossRef]
54. Ledentsov, N., Jr.; Chorchos, L.; Makarov, O.Y.; Shchukin, V.A.; Kalosha, V.P.; Kropp, J.R.; Turkiewicz, J.P.; Kottke, C.; Jungnickel, V.; Freund, R.; et al. Serial data transmission at 224 Gbit/s applying directly modulated 850 and 910 nm VCSELs. *Electron. Lett.* **2021**, *57*, 735–737. [CrossRef]
55. Kao, H.Y.; Tsai, C.T.; Leong, S.F.; Peng, C.Y.; Chi, Y.C.; Huang, J.J.; Kuo, H.C.; Shih, T.T.; Jou, J.J.; Cheng, W.H.; et al. Comparison of single-/few-/multi-mode 850 nm VCSELs for optical OFDM transmission. *Opt. Express* **2017**, *25*, 16347–16363. [CrossRef] [PubMed]
56. Kao, H.Y.; Huang, C.Y.; Peng, C.Y.; Tsai, C.T.; Wang, H.Y.; Leong, S.F.; Kuo, H.C.; Wu, C.H.; Lin, G.R. Single-mode VCSEL for Nearly 100-Gbit/s QAM-OFDM transmission over 100-m OM4 multi-mode fiber. In Proceedings of the CLEO Pacific Rim Conference 2018, Hong Kong, China, 29 July–3 August 2018; Optical Society of America: Washington, DC, USA, 2018; p. W3A.12. [CrossRef]
57. Wu, W.L.; Huang, C.Y.; Wang, H.Y.; Lin, Y.H.; Wu, C.H.; Kuo, H.C.; Cheng, W.H.; Wu, C.H.; Feng, M.; Lin, G.R. VCSEL with bi-layer oxidized aperture enables 140-Gbit/s OFDM Transmission over 100-m-long OM5 MMF. In Proceedings of the Optical Fiber Communication Conference (OFC) 2019, San Diego, CA, USA, 3–7 March 2019; Optical Society of America: Washington, DC, USA, 2019; p. Tu3A.3. [CrossRef]

58. Lo, W.C.; Wu, W.L.; Peng, C.Y.; Wang, H.Y.; Tsai, C.T.; Su, B.; Wu, C.H.; Lin, G.R. Multimode VCSEL Enables Multi-Data-Format Encoding up to 124 Gbit/s. In Proceedings of the Conference on Lasers and Electro-Optics, Washington, DC, USA, 10–15 May 2020; Optical Society of America: Washington, DC, USA, 2020; p. STu4M.5. [CrossRef]
59. Wu, C.H.; Huang, T.Y.; Qiu, J.; Fu, W.; Peng, C.Y.; Shih, T.T.; Huang, J.J.; Kuo, H.C.; Lin, G.R.; Cheng, W.H.; et al. 50 Gb/s Error-Free Data Transmission Using a NRZ-OOK Modulated 850 nm VCSEL. In Proceedings of the 2018 European Conference on Optical Communication (ECOC), Rome, Italy, 23–27 September 2018; pp. 1–3. [CrossRef]
60. Huang, T.Y.; Qiu, J.; Wu, C.H.; Cheng, H.T.; Feng, M.; Kuo, H.C.; Wu, C.H. A NRZ-OOK Modulated 850-nm VCSEL with 54 Gb/s Error-Free Data Transmission. In Proceedings of the 2019 Conference on Lasers and Electro-Optics Europe European Quantum Electronics Conference (CLEO/Europe-EQEC), Munich, Germany, 23–27 June 2019; p. 1. [CrossRef]
61. Chorchos, L.; Ledentsov, N.; Kropp, J.R.; Shchukin, V.A.; Kalosha, V.P.; Lewandowski, A.; Turkiewicz, J.P.; Ledentsov, N.N. Energy Efficient 850 nm VCSEL Based Optical Transmitter and Receiver Link Capable of 80 Gbit/s NRZ Multi-Mode Fiber Data Transmission. *J. Light. Technol.* **2020**, *38*, 1747–1752. [CrossRef]
62. Haglund, E.; Westbergh, P.; Gustavsson, J.S.; Haglund, E.P.; Larsson, A.; Geen, M.; Joel, A. 30 GHz bandwidth 850 nm VCSEL with sub-100 fJ/bit energy dissipation at 25–50 Gbit/s. *Electron. Lett.* **2015**, *51*, 1096–1098. [CrossRef]
63. Wang, J.; Murty, M.V.R.; Feng, Z.W.; Joyo, S.T.; Sridhara, A.; Cai, X.; Harren, A.L.; Leong, N.; Koh, G.H.; Cheng, A.N.; et al. 100Gb/s PAM4 oxide VCSEL development progress at Broadcom. In *Vertical-Cavity Surface-Emitting Lasers XXIV*; Graham, L.A., Lei, C., Eds.; International Society for Optics and Photonics, SPIE: Bellingham, WA, USA, 2020; Volume 11300, pp. 84–89. [CrossRef]
64. Ledentsov, N.; Chorchos, L.; Makarov, O.; Kropp, J.R.; Shchukin, V.A.; Kalosha, V.P.; Turkiewicz, J.P.; Ledentsov, N.N. Narrow spectrum VCSEL development for high performance 100G transceivers and increased transmission distance over multimode fiber. In *Vertical-Cavity Surface-Emitting Lasers XXV*; Lei, C., Choquette, K.D., Eds.; International Society for Optics and Photonics, SPIE: Bellingham, WA, USA, 2021; Volume 11704, pp. 78–84. [CrossRef]
65. Yang, Y.C.; Cheng, H.T.; Wu, C.H. 30 GHz Highly Damped Oxide Confined Vertical-Cavity Surface-Emitting Laser. In Proceedings of the 2021 IEEE Photonics Conference (IPC), Vancouver, BC, Canada, 18–21 October 2021; pp. 1–2. [CrossRef]
66. Maki, J.J. Pivotal Issues for 400 Gb/s Ethernet. Available online: https://www.ieee802.org/3/bs/public/14_05/maki_3bs_01a_0514.pdf (accessed on 5 January 2022).
67. Lee, J.; Chiang, P.C.; Peng, P.J.; Chen, L.Y.; Weng, C.C. Design of 56 Gb/s NRZ and PAM4 SerDes Transceivers in CMOS Technologies. *IEEE J.-Solid-State Circuits* **2015**, *50*, 2061–2073. [CrossRef]
68. Li, M.J.; Li, K.; Chen, X.; Mishra, S.K.; Juarez, A.A.; Hurley, J.E.; Stone, J.S.; Wang, C.H.; Cheng, H.T.; Wu, C.H.; et al. Single-Mode VCSEL Transmission for Short Reach Communications. *J. Light. Technol.* **2021**, *39*, 868–880. [CrossRef]
69. Kao, H.Y.; Chi, Y.C.; Peng, C.Y.; Leong, S.F.; Chang, C.K.; Wu, Y.C.; Shih, T.T.; Huang, J.J.; Kuo, H.C.; Cheng, W.H.; et al. Modal Linewidth Dependent Transmission Performance of 850-nm VCSELs With Encoding PAM-4 Over 100-m MMF. *IEEE J. Quantum Electron.* **2017**, *53*, 1–8. [CrossRef]
70. Qiu, J.; Yu, X.; Feng, M. 85 °C Operation of Single-Mode 850 nm VCSELs for High Speed Error-Free Transmission up to 1 km in OM4 Fiber. In Proceedings of the Optical Fiber Communication Conference (OFC) 2019, San Diego, CA, USA, 3–7 March 2019; Optical Society of America: Washington, DC, USA, 2019; p. W3A.4. [CrossRef]
71. Peng, C.Y.; Qiu, J.; Huang, T.Y.; Wu, C.H.; Feng, M.; Wu, C.H. 850-nm Single-Mode Vertical-Cavity Surface-Emitting Lasers for 40 Gb/s Error-Free Transmission up to 500 m in OM4 Fiber. *IEEE Electron Device Lett.* **2020**, *41*, 84–86. [CrossRef]
72. Huang, C.Y.; Tsai, C.T.; Weng, J.H.; Cheng, C.H.; Wang, H.Y.; Wu, C.H.; Feng, M.; Lin, G.R. Temperature and Noise Dependence of Tri-Mode VCSEL Carried 120-Gbit/s QAM-OFDM Data in Back-to-Back and OM5-MMF Links. *J. Light. Technol.* **2020**, *38*, 6746–6758. [CrossRef]
73. Haglund, E.; Haglund, Å.; Gustavsson, J.S.; Kögel, B.; Westbergh, P.; Larsson, A. Reducing the spectral width of high speed oxide confined VCSELs using an integrated mode filter. In *Vertical-Cavity Surface-Emitting Lasers XVI*; Lei, C., Choquette, K.D., Eds.; International Society for Optics and Photonics, SPIE: Bellingham, WA, USA, 2012; Volume 8276, pp. 171–178. [CrossRef]
74. Orenstein, M.; Stoffel, N.; Von Lehmen, A.; Harbison, J.; Florez, L. Efficient continuous wave operation of vertical-cavity semiconductor lasers using buried-compensation layers to optimize current flow. *Appl. Phys. Lett.* **1991**, *59*, 31–33. [CrossRef]
75. Unold, H.; Mahmoud, S.; Jager, R.; Grabherr, M.; Michalzik, R.; Ebeling, K. Large-area single-mode VCSELs and the self-aligned surface relief. *IEEE J. Sel. Top. Quantum Electron.* **2001**, *7*, 386–392. [CrossRef]
76. Gustavsson, J.; Haglund, A.; Bengtsson, J.; Modh, P.; Larsson, A. Dynamic behavior of fundamental-mode stabilized VCSELs using a shallow surface relief. *IEEE J. Quantum Electron.* **2004**, *40*, 607–619. [CrossRef]
77. Song, D.S.; Kim, S.H.; Park, H.G.; Kim, C.K.; Lee, Y.H. Single-fundamental-mode photonic-crystal Vertical-Cavity Surface-Emitting Lasers. *Appl. Phys. Lett.* **2002**, *80*, 3901–3903. [CrossRef]
78. Danner, A.; Kim, T.; Choquette, K. Single fundamental mode photonic crystal vertical cavity laser with improved output power. *Electron. Lett.* **2005**, *41*, 325–326. [CrossRef]
79. Yang, Y.J.; Dziura, T.G.; Bardin, T.; Wang, S.C.; Fernandez, R. Continuous-wave single-transverse-mode vertical-cavity surface-emitting lasers fabricated by helium Implantation and zinc diffusion. *Electron. Lett.* **1992**, *28*, 274–276. [CrossRef]
80. Shi, J.W.; Chen, C.C.; Wu, Y.S.; Guol, S.H.; Kuo, C.; Yang, Y.J. High-Power and High-Speed Zn-Diffusion Single Fundamental-Mode Vertical-Cavity Surface-Emitting Lasers at 850-nm Wavelength. *IEEE Photonics Technol. Lett.* **2008**, *20*, 1121–1123. [CrossRef]

81. Shi, J.W.; Yan, J.C.; Wun, J.M.; Chen, J.; Yang, Y.J. Oxide-Relief and Zn-Diffusion 850-nm Vertical-Cavity Surface-Emitting Lasers With Extremely Low Energy-to-Data-Rate Ratios for 40 Gbit/s Operations. *IEEE J. Sel. Top. Quantum Electron.* **2013**, *19*, 7900208. [CrossRef]
82. Shi, J.W.; Wei, Z.R.; Chi, K.L.; Jiang, J.W.; Wun, J.M.; Lu, I.C.; Chen, J.; Yang, Y.J. Single-Mode, High-Speed, and High-Power Vertical-Cavity Surface-Emitting Lasers at 850 nm for Short to Medium Reach (2 km) Optical Interconnects. *J. Light. Technol.* **2013**, *31*, 4037–4044. [CrossRef]
83. Shi, J.W.; Wei, C.C.; Chen, J.; Ledentsov, N.N.; Yang, Y.J. Single-mode 850-nm vertical-cavity surface-emitting lasers with Zn-diffusion and oxide-relief apertures for >50 Gbit/sec OOK and 4-PAM transmission. In *Vertical-Cavity Surface-Emitting Lasers XXI*; Choquette, K.D., Lei, C., Eds.; International Society for Optics and Photonics, SPIE: Bellingham, WA, USA, 2017; Volume 10122, pp. 99–108. [CrossRef]
84. Peng, C.Y.; Cheng, H.T.; Kuo, H.C.; Wu, C.H. Design and Optimization of VCSELs for up to 40-Gb/s Error-Free Transmission Through Impurity-Induced Disordering. *IEEE Trans. Electron Devices* **2020**, *67*, 1041–1046. [CrossRef]
85. Lee, S.Y.; Chen, X.; Lo, W.C.; Li, K.; Wang, C.H.; Tsai, C.T.; Cheng, C.H.; Wu, C.H.; Kuo, H.C.; Li, M.J.; et al. 850-nm Dual-Mode VCSEL Carried 53-Gbps NRZ- OOK Transmission in 100-m Graded-Index Single-Mode Fiber. In Proceedings of the Optical Fiber Communication Conference (OFC) 2021, Washington, DC, USA, 6–11 June 2021; Optical Society of America: Washington, DC, USA, 2021; p. Tu5C.3. [CrossRef]
86. Cheng, C.L.; Ledentsov, N.; Agustin, M.; Kropp, J.R.; Ledentsov, N.N.; Khan, Z.; Shi, J.W. Ultra-Fast Zn-Diffusion/Oxide-Relief 940 nm VCSELs. In Proceedings of the Optical Fiber Communication Conference (OFC) 2019, San Diego, CA, USA, 3–7 March 2019; Optical Society of America: Washington, DC, USA, 2019; p. W3A.2. [CrossRef]
87. Wang, H.L.; Qiu, J.; Yu, X.; Fu, W.; Feng, M. The Modal Effect of VCSELs on Transmitting Data Rate Over Distance in OM4 Fiber. *IEEE J. Quantum Electron.* **2020**, *56*, 1–6. [CrossRef]
88. Lu, D.; Ahn, J.; Huang, H.; Deppe, D.G. All-epitaxial mode-confined vertical-cavity surface-emitting laser. *Appl. Phys. Lett.* **2004**, *85*, 2169–2171. [CrossRef]
89. Zhao, G.; Deppe, D. Thermal performance of oxide-free lithographic VCSELs. In Proceedings of the IEEE Photonic Society 24th Annual Meeting, Arlington, VA, USA, 9–13 October 2011; pp. 915–916. [CrossRef]
90. Piprek, J. *Semiconductor Optoelectronic Devices: Introduction to Physics and Simulation*; Elsevier: Amsterdam, The Netherlands, 2013.
91. Haglund, E.P.; Westbergh, P.; Gustavsson, J.S.; Larsson, A. Impact of Damping on High-Speed Large Signal VCSEL Dynamics. *J. Light. Technol.* **2015**, *33*, 795–801. [CrossRef]
92. Cheng, J.; Dutta, N.K. *Vertical-Cavity Surface-Emitting Lasers: Technology and Applications*; CRC Press: Boca Raton, FL, USA, 2000; Volume 10.
93. Michalzik, R. *VCSELs: Fundamentals, Technology and Applications of Vertical-Cavity Surface-Emitting Lasers*; Springer: Berlin/Heidelberg, Germany, 2012.
94. Larsson, A.; Gustavsson, J.S.; Westbergh, P.; Haglund, E.; Haglund, E.P.; Simpanen, E.; Lengyel, T.; Szczerba, K.; Karlsson, M. VCSEL design and integration for high-capacity optical interconnects. In *Optical Interconnects XVII*; Schröder, H., Chen, R.T., Eds.; International Society for Optics and Photonics, SPIE: Bellingham, WA, USA, 2017; Volume 10109, pp. 129–134. [CrossRef]
95. Bond, A.; Dapkus, P.; O'brien, J. Aperture placement effects in oxide-defined vertical-cavity surface-emitting lasers. *IEEE Photonics Technol. Lett.* **1998**, *10*, 1362–1364. [CrossRef]
96. Healy, S.B.; O'Reilly, E.P.; Gustavsson, J.S.; Westbergh, P.; Haglund, A.; Larsson, A.; Joel, A. Active Region Design for High-Speed 850-nm VCSELs. *IEEE J. Quantum Electron.* **2010**, *46*, 506–512. [CrossRef]
97. Zhao, B.; Chen, T.; Yariv, A. The extra differential gain enhancement in multiple-quantum-well lasers. *IEEE Photonics Technol. Lett.* **1992**, *4*, 124–126. [CrossRef]
98. Liu, Y.; Ng, W.C.; Choquette, K.; Hess, K. Numerical investigation of self-heating effects of oxide-confined vertical-cavity surface-emitting lasers. *IEEE J. Quantum Electron.* **2005**, *41*, 15–25. [CrossRef]
99. AL-Omari, A.N.; Lear, K.L. Polyimide-planarized vertical-cavity surface-emitting lasers with 17.0-GHz bandwidth. *IEEE Photonics Technol. Lett.* **2004**, *16*, 969–971. [CrossRef]
100. Chang, Y.C.; Coldren, L.A. Efficient, High-Data-Rate, Tapered Oxide-Aperture Vertical-Cavity Surface-Emitting Lasers. *IEEE J. Sel. Top. Quantum Electron.* **2009**, *15*, 704–715. [CrossRef]
101. AL-Omari, A.N.; AL-Kofahi, I.K.; Lear, K.L. Fabrication, performance and parasitic parameter extraction of 850 nm high-speed vertical-cavity lasers. *Semicond. Sci. Technol.* **2009**, *24*, 095024. [CrossRef]
102. Mutig, A.; Fiol, G.; Potschke, K.; Moser, P.; Arsenijevic, D.; Shchukin, V.A.; Ledentsov, N.N.; Mikhrin, S.S.; Krestnikov, I.L.; Livshits, D.A.; et al. Temperature-Dependent Small-Signal Analysis of High-Speed High-Temperature Stable 980-nm VCSELs. *IEEE J. Sel. Top. Quantum Electron.* **2009**, *15*, 679–686. [CrossRef]
103. Wu, C.H.; Tan, F.; Wu, M.K.; Feng, M.; Holonyak, N. The effect of microcavity laser recombination lifetime on microwave bandwidth and eye-diagram signal integrity. *J. Appl. Phys.* **2011**, *109*, 053112. [CrossRef]
104. Hamad, W.; Wanckel, S.; Hofmann, W.H.E. Small-Signal Analysis of Ultra-High-Speed Multi-Mode VCSELs. *IEEE J. Quantum Electron.* **2016**, *52*, 1–11. [CrossRef]
105. Hamad, W.; Bou Sanayeh, M.; Hamad, M.M.; Hofmann, W.H.E. Impedance Characteristics and Chip-Parasitics Extraction of High-Performance VCSELs. *IEEE J. Quantum Electron.* **2020**, *56*, 1–11. [CrossRef]

106. Gębski, M.; Wong, P.S.; Riaziat, M.; Lott, J.A. 30 GHz bandwidth temperature stable 980 nm vertical-cavity surface-emitting lasers with AlAs/GaAs bottom distributed Bragg reflectors for optical data communication. *J. Phys. Photonics* **2020**, *2*, 035008. [CrossRef]
107. Larisch, G.; Tian, S.; Bimberg, D. Optimization of VCSEL photon lifetime for minimum energy consumption at varying bit rates. *Opt. Express* **2020**, *28*, 18931–18937. [CrossRef]
108. Feng, M.; Wu, C.H.; Holonyak, N. Oxide-Confined VCSELs for High-Speed Optical Interconnects. *IEEE J. Quantum Electron.* **2018**, *54*, 1–15. [CrossRef]
109. van Eisden, J.; Yakimov, M.; Tokranov, V.; Varanasi, M.; Mohammed, E.M.; Young, I.A.; Oktyabrsky, S. Modulation properties of VCSEL with intracavity modulator. In *Vertical-Cavity Surface-Emitting Lasers XI*; Choquette, K.D., Guenter, J.K., Eds.; International Society for Optics and Photonics, SPIE: Bellingham, WA, USA, 2007; Volume 6484, pp. 84–93. [CrossRef]
110. Kojima, K.; Morgan, A.; Mullally, T.; Guth, G.D.; Focht, M.W.; Leibenguth, K.E.; Asom, M.T. Reduction of p-doped mirror electrical resistance of GaAs/AIGaAs vertical-cavity surface-emitting lasers by delta-doping. In Proceedings of the Conference on Lasers and Electro-Optics, Baltimore, MD, USA, 2–7 May 1993; Optical Society of America: Washington, DC, USA, 1993; pp. 1771–1772. [CrossRef]
111. Peters, M.G.; Thibeault, B.J.; Young, D.B.; Scott, J.W.; Peters, F.H.; Gossard, A.C.; Coldren, L.A. Band-gap engineered digital alloy interfaces for lower resistance vertical-cavity surface-emitting lasers. *Appl. Phys. Lett.* **1993**, *63*, 3411–3413. [CrossRef]
112. Liu, Y.; Ng, W.C.; Oyafuso, F.; Klein, B.; Hess, K. Simulating the modulation response of VCSELs: The effects of diffusion capacitance and spatial hole-burning. *Optoelectron. IEE Proc.* **2002**, *149*, 182–188. [CrossRef]
113. Nishiyama, N.; Arai, M.; Shinada, S.; Suzuki, K.; Koyama, F.; Iga, K. Multi-oxide layer structure for single-mode operation in Vertical-Cavity Surface-Emitting Lasers. *IEEE Photonics Technol. Lett.* **2000**, *12*, 606–608. [CrossRef]
114. Azuchi, M.; Jikutani, N.; Arai, M.; Kondo, T.; Koyama, F. Multioxide layer vertical-cavity surface-emitting lasers with improved modulation bandwidth. In Proceedings of the CLEO/Pacific Rim 2003, the 5th Pacific Rim Conference on Lasers and Electro-Optics (IEEE Cat. No.03TH8671), Taipei, Taiwan, 15–19 December 2003; Volume 1, p. 163. [CrossRef]
115. Chang, Y.-C.; Wang, C.S. High-efficiency, high-speed VCSELs with 35 Gbit/s error-free operation. *Electron. Lett.* **2007**, *43*, 1022–1023. [CrossRef]
116. Yang, Y.C.; Cheng, H.T.; Wu, C.H. Ultra-fast and Highly Efficient 850-nm VCSELs for Next-gen PAM-4 Transceivers. In Proceedings of the Asia Communications and Photonics Conference 2021, Shanghai, China, 24–27 October 2021; Chang-Hasnain, C., Willner, A., Shieh, W., Shum, P., Su, Y., Li, G., Eggleton, B., Essiambre, R., Dai, D., Ma, D., Eds.; Optical Society of America: Washington, DC, USA, 2021; p. W3D.4. [CrossRef]
117. Kuchta, D.; Pepeljugoski, P.; Kwark, Y. VCSEL modulation at 20 Gb/s over 200 m of multimode fiber using a 3.3 V SiGe laser driver IC. In Proceedings of the 2001 Digest of LEOS Summer Topical Meetings: Advanced Semiconductor Lasers and Applications/Ultraviolet and Blue Lasers and Their Applications/Ultralong Haul DWDM Transmission and Networking/WDM Compo, Copper Mountain, CO, USA, 30 July–1 August 2001; p. 2. [CrossRef]
118. Westbergh, P.; Gustavsson, J.S.; Kögel, B.; Haglund, Å.; Larsson, A.; Mutig, A.; Nadtochiy, A.; Bimberg, D.; Joel, A. 40 Gbit/s error-free operation of oxide-confined 850 nm VCSEL. *Electron. Lett.* **2010**, *46*, 1014–1016. [CrossRef]
119. Westbergh, P.; Safaisini, R.; Haglund, E.; Gustavsson, J.S.; Larsson, A.; Joel, A. High-speed 850-nm VCSELs with 28 GHz modulation bandwidth for short reach communication. In *Vertical-Cavity Surface-Emitting Lasers XVII*; Choquette, K.D., Guenter, J.K., Eds.; International Society for Optics and Photonics, SPIE: Bellingham, WA, USA, 2013; Volume 8639, pp. 251–256. [CrossRef]
120. Westbergh, P.; Gustavsson, J.S.; Haglund, A.; Sunnerud, H.; Larsson, A. Large aperture 850 nm VCSELs operating at bit rates up to 25 Gbit/s. *Electron. Lett.* **2008**, *44*, 907–908. [CrossRef]
121. Tan, F.; Wu, C.H.; Feng, M.; Holonyak, N. Energy efficient microcavity lasers with 20 and 40 Gb/s data transmission. *Appl. Phys. Lett.* **2011**, *98*, 191107. [CrossRef]
122. Kuchta, D.M.; Rylyakov, A.V.; Schow, C.L.; Proesel, J.E.; Baks, C.; Kocot, C.; Graham, L.; Johnson, R.; Landry, G.; Shaw, E.; et al. A 55Gb/s directly modulated 850nm VCSEL-based optical link. *IEEE Photonics Conf.* **2012**, *2012*, 1–2. [CrossRef]
123. Szczerba, K.; Westbergh, P.; Karlsson, M.; Andrekson, P.; Larsson, A. 60 Gbits error-free 4-PAM operation with 850 nm VCSEL. *Electron. Lett.* **2013**, *49*, 953–955. [CrossRef]
124. Westbergh, P.; Haglund, E.; Haglund, E.; Safaisini, R.; Gustavsson, J.; Larsson, A. High-speed 850 nm VCSELs operating error free up to 57 Gbit/s. *Electron. Lett.* **2013**, *49*, 1021–1023. [CrossRef]
125. Chi, K.L.; Jiang, J.W.; Yen, J.L.; Lu, I.C.; Kuo, H.C.; Chen, J.J.; Yang, Y.J.; Wei, C.C.; Shi, J.W. Energy Efficient 850 nm Vertical-Cavity Surface-Emitting Lasers with Extremely Low Driving-Current Density for >40 Gbit/sec Error-Free Transmissions from RT to 85 °C. In Proceedings of the Optical Fiber Communication Conference, Los Angeles, CA, USA, 22–26 March 2015; Optical Society of America: Washington, DC, USA, 2015; p. M2D.6. [CrossRef]
126. Chi, K.L.; Yen, J.L.; Wun, J.M.; Jiang, J.W.; Lu, I.C.; Chen, J.; Yang, Y.J.; Shi, J.W. Strong Wavelength Detuning of 850 nm Vertical-Cavity Surface-Emitting Lasers for High-Speed (>40 Gbit/s) and Low-Energy Consumption Operation. *IEEE J. Sel. Top. Quantum Electron.* **2015**, *21*, 470–479. [CrossRef]
127. Giovane, L.M.; Wang, J.; Murty, M.V.R.; Harren, A.L.; Chang, H.H.; Wang, C.; Hui, D.; Feng, Z.W.; Fanning, T.R.; Sridhara, A.; et al. Volume Manufacturable High speed 850nm VCSEL for 100G Ethernet and Beyond. In Proceedings of the Optical Fiber Communication Conference, Anaheim, CA, USA, 20–22 March 2016; Optical Society of America: Washington, DC, USA, 2016; p. Tu3D.5. [CrossRef]

128. Liu, M.; Wang, C.Y.; Feng, M.; Holonyak, N. 50 Gb/s Error-Free Data Transmission of 850 nm Oxide-Confined VCSELs. In Proceedings of the Optical Fiber Communication Conference, Anaheim, CA, USA, 20–22 March 2016; Optical Society of America: Washington, DC, USA, 2016; p. Tu3D.2. [CrossRef]
129. Liu, M.; Wang, C.Y.; Feng, M.; Holonyak, N. Advanced Development of 850 nm Oxide-Confined VCSELs with 57 Gb/s Error-Free Data Transmission. In Proceedings of the Government Microcircuit Applications Critical Technology Conference (GOMACTech), Orlando, FL, USA, 14–17 March 2016.
130. Wang, J.; Murty, M.V.R.; Wang, C.; Hui, D.; Harren, A.L.; Chang, H.H.; Feng, Z.W.; Fanning, T.R.; Sridhara, A.; Joyo, S.T.; et al. 50Gb/s PAM-4 oxide VCSEL development progress at Broadcom. In *Vertical-Cavity Surface-Emitting Lasers XXI*; Choquette, K.D., Lei, C., Eds.; International Society for Optics and Photonics, SPIE: Bellingham, WA, USA, 2017; Volume 10122, pp. 1–6. [CrossRef]
131. Ledentsov, N., Jr.; Agustin, M.; Chorchos, L.; Kropp, J.R.; Shchukin, V.A.; Kalosha, V.P.; Koepp, M.; Caspar, C.; Turkiewicz, J.P.; Ledentsov, N.N. Energy efficient 850-nm VCSEL based optical transmitter and receiver link capable of 56 Gbit/s NRZ operation. In *Vertical-Cavity Surface-Emitting Lasers XXIII*; Choquette, K.D., Graham, L.A., Eds.; International Society for Optics and Photonics, SPIE: Bellingham, WA, USA, 2019; Volume 10938, pp. 77–84. [CrossRef]
132. Hecht, U.; Ledentsov, N.; Chorchos, L.; Scholz, P.; Schulz, P.; Turkiewicz, J.P.; Ledentsov, N.N.; Gerfers, F. 120Gbit/s multi-mode fiber transmission realized with feed forward equalization using 28GHz 850nm VCSELs. In Proceedings of the 45th European Conference on Optical Communication (ECOC 2019), Dublin, Ireland, 22–26 September 2019; IET: London, UK, 2019; pp. 1–4. [CrossRef]
133. Murty, M.V.R.; Wang, J.; Harren, A.L.; Cheng, A.N.; Dolfi, D.W.; Feng, Z.W.; Sridhara, A.; Joyo, S.T.; Chu, J.; Giovane, L.M. Development and Characterization of 100 Gb/s Data Communication VCSELs. *IEEE Photonics Technol. Lett.* **2021**, *33*, 812–815. [CrossRef]
134. Qiu, J.; Wu, D.; Wang, H.L.; Feng, M.; Yu, X. Advanced Single-Mode 850 nm VCSELs for Record NRZ and PAM4 Data Rate on SMF-28 Fiber up to 1 km. In Proceedings of the Optical Fiber Communication Conference (OFC) 2021, Washington, DC, USA, 6–11 June 2021; Optical Society of America: Washington, DC, USA, 2021; p. Tu5C.2. [CrossRef]
135. Westbergh, P.; Gustavsson, J.S.; Haglund, Å.; Larsson, A.; Hopfer, F.; Bimberg, D.; Joel, A. 32 Gb/s transmission experiments using high speed 850 nm VCSELs. In Proceedings of the 2009 Conference on Lasers and Electro-Optics and 2009 Conference on Quantum electronics and Laser Science Conference, Baltimore, MD, USA, 31 May–5 June 2009; Optical Society of America: Washington, DC, USA, 2009; pp. 1–2. [CrossRef]
136. Wolf, P.; Moser, P.; Larisch, G.; Li, H.; Lott, J.; Bimberg, D. Energy efficient 40 Gbit/s transmission with 850 nm VCSELs at 108 fJ/bit dissipated heat. *Electron. Lett.* **2013**, *49*, 666–667. [CrossRef]
137. Stepniak, G.; Lewandowski, A.; Kropp, J.; Ledentsov, N.; Shchukin, V.; Ledentsov, N., Jr.; Schaefer, G.; Agustin, M.; Turkiewicz, J. 54 Gbit/s OOK transmission using single-mode VCSEL up to 2.2 km MMF. *Electron. Lett.* **2016**, *52*, 633–635. [CrossRef]
138. Motaghiannezam, S.; Lyubomirsky, I.; Daghighian, H.; Kocot, C.; Gray, T.; Tatum, J.; Amezcua-Correa, A.; Bigot-Astruc, M.; Molin, D.; Achten, F.; et al. 180 Gbps PAM4 VCSEL Transmission over 300m Wideband OM4 Fibre. In Proceedings of the Optical Fiber Communication Conference, Anaheim, CA, USA, 20–22 March 2016; Optical Society of America: Washington, DC, USA, 2016; p. Th3G.2. [CrossRef]
139. Castro, J.M.; Pimpinella, R.; Kose, B.; Huang, Y.; Lane, B.; Szczerba, K.; Westbergh, P.; Lengyel, T.; Gustavsson, J.S.; Larsson, A.; et al. 50 Gb/s 4-PAM over 200 m of High Bandwidth MMF using a 850 nm VCSEL. In Proceedings of the Optical Fiber Communication Conference, Los Angeles, CA, USA, 22–26 March 2015; Optical Society of America: Washington, DC, USA, 2015; p. W1D.1. [CrossRef]
140. Kao, H.Y.; Tsai, C.T.; Leong, S.F.; Peng, C.Y.; Chi, Y.C.; Wang, H.Y.; Kuo, H.C.; Wu, C.H.; Cheng, W.H.; Lin, G.R. Single-mode VCSEL for pre-emphasis PAM-4 transmission up to 64 Gbit/s over 100–300 m in OM4 MMF. *Photonics Res.* **2018**, *6*, 666–673. [CrossRef]
141. Yang, Y.; Dziura, T.; Wang, S.; Du, G.; Wang, S. Single-mode operation of mushroom structure surface emitting lasers. *IEEE Photonics Technol. Lett.* **1991**, *3*, 9–11. [CrossRef]
142. Broadcom Inc. 112-Gb/s (56-GBd) 850-nm 1 × 4 Array Oxide VCSEL. Available online: https://www.broadcom.com/products/fiber-optic-modules-components/components-broadband/short-reach-gaas-die/lasers/afcd-v84lp/ (accessed on 5 January 2022).
143. VI Systems GmbH. VIS-Datasheet-V50-850C. Available online: https://v-i-systems.com/wp-content/uploads/2020/12/VIS-Datasheet-V50-850C-1.pdf (accessed on 5 January 2022).
144. Shannon, C. Communication in the Presence of Noise. *Proc. IRE* **1949**, *37*, 10–21. [CrossRef]
145. Moser, P.; Hofmann, W.; Wolf, P.; Lott, J.A.; Larisch, G.; Payusov, A.; Ledentsov, N.N.; Bimberg, D. 81 fJ/bit energy-to-data ratio of 850 nm vertical-cavity surface-emitting lasers for optical interconnects. *Appl. Phys. Lett.* **2011**, *98*, 231106. [CrossRef]
146. Moser, P.; Lott, J.A.; Bimberg, D. Energy Efficiency of Directly Modulated Oxide-Confined High Bit Rate 850-nm VCSELs for Optical Interconnects. *IEEE J. Sel. Top. Quantum Electron.* **2013**, *19*, 1702212. [CrossRef]
147. Szczerba, K.; Westbergh, P.; Gustavsson, J.S.; Karlsson, M.; Andrekson, P.A.; Larsson, A. Energy Efficiency of VCSELs in the Context of Short-Range Optical Links. *IEEE Photonics Technol. Lett.* **2015**, *27*, 1749–1752. [CrossRef]